INVESTIGATION OF THE GEOTHERMAL POTENTIAL IN THE EASTERN SIDE OF OLKARIA DOMES USING MAGNETOTELLURIC METHOD

MELINA NABWIRE

MASTER OF SCIENCE IN
APPLIED GEOPHYSICS

JOMO KENYATTA UNIVERSITY
OF
AGRICULTURE AND TECHNOLOGY

2026

Investigation of the Geothermal Potential in the Eastern Side of Olkaria Domes Using Magnetotelluric Method

Melina Nabwire

A Thesis Submitted in Partial Fulfillment of the Requirements for the Degree of Master of Science in Applied Geophysics (Geothermal Science) of the Jomo Kenyatta University of Agriculture and Technology

2026

DECLARATION

This thesis is my original work and has not been presented for a degree at any other University

Signature……..Date…….

Melina Nabwire

This thesis has been submitted for examination with our approval as the University Supervisors

Signature……..Date…….

Dr. Justus Mutuku Maithya, PhD

JKUAT, Kenya

Signature……..Date…….

Dr. James Mwendwa Munyithya, PhD

JKUAT, Kenya

DEDICATION

This work is dedicated to my parents and siblings who have always believed in me, encouraged my dreams, and provided endless wisdom and strength. I would not have reached this milestone without you.

ACKNOWLEDGEMENT

First and foremost, I wish to thank the Almighty God for the gift of life, a sound mind, knowledge, and sustenance throughout my research.

I want to express my deepest gratitude to my principal Supervisors, Dr. Justus Maithya and Dr. James Munyithya, for their invaluable guidance, expertise and unwavering support throughout this research. Your insightful feedback and encouragement were instrumental in the completion of this work.

My heartfelt gratitude goes to Professor Nicholas Mariita of Dedan Kimathi University for his encouragement and support throughout my Master's journey. Your guidance and belief in me have been instrumental in my growth and confidence. I'm grateful for the opportunity to have learned from you. Thank you for being an exceptional mentor and role model.

I want to thank Professor John Gitonga Githiri whose mentorship and encouragement have profoundly influenced my academic journey and career path. Thank you for guiding me with wisdom, kindness, and dedication. I will always be grateful for the impact you have had on my life and career.

To my classmate Otanga Wesonga Answari and my friends; Eunice Wachira, Sheila Korir, Chepsang Jepchumba Caroline and Suzan Wanjiku Kamau, your encouragement and friendship have made this journey memorable and enjoyable.

I acknowledge Kenya Electricity Generating Company Ltd (KenGen) for providing MT data for this research. To African Development Bank (AFDB) and the Ministry of Education, I express my sincere gratitude for the Master's scholarship awarded to me. I am grateful for the opportunity, which has enabled me to pursue my academic goals and enhance my skills. Thank you for the support and investment in my future.

TABLE OF CONTENTS

LIST OF FIGURES

LIST OF APPENDICES

ACRONYMS AND ABBREVIATIONS

EARS	East African Rift System
GOVC	The Great Olkaria Volcanic Complex
GPS	Global Positioning System
MT	Magnetotelluric
OW	Olkaria Well
TE	Transverse Electric
TEM	Transient Electromagnetic
TM	Transverse Magnetic
1D	One – Dimensional
2D	Two – Dimensional
DC	Direct current
BP	Before Present
EM	Electromagnetic
GPS	Global Positioning System
EDI	Electronic data interchange
UNU	United Nations University
GTP	Geothermal Training Programme

GDC	Geothermal Development Company
TDEM	Time – Domain Electromagnetic
NE	North East
SW	South West

LIST OF SYMBOLS

σ	Conductivity
μ	Magnetic permeability
ε	Electrical permittivity
η	Electric charge density
Ω	Ohm
H	Magnetic intensity
B	Magnetic flux density
T	Periodic time
ω	Angular frequency
Z	Impedance
Ωm	Ohm – meter
H_X	Magnetic component in the north - south direction
H_Y	Magnetic component in the east - west direction
H_Z	Magnetic component into the ground surface
Ex	Electric field in the x- direction
E_Y	Electric field in the y- direction

H/m	Henry per meter
μ_o	Permeability of free space
ρ	Resistivity

ABSTRACT

High-temperature geothermal resources are commonly found along rift margins due to the intrusion of magma into the shallow crust, as is evident in the Kenyan Rift Valley. Among the volcanic centers in this region, Olkaria stands out as the most extensively explored and is currently in an advanced stage of geothermal development. Despite its success as a major energy source, further investigations are on-going to optimize the development of its geothermal fields. In particular, the area east of the Olkaria domes remains largely unexplored, with only one well, OW-922, drilled to date. Unfortunately, this well failed to sustain discharge during testing. This highlights the need for a comprehensive study to assess the geothermal potential and improve the understanding of the field in this region. To address this, both 2D and 3D magnetotelluric (MT) inversions were performed using data from 50 soundings. The obtained models were analysed to map the subsurface structures influencing the geothermal system on the eastern side of the domes. A spatial median filter was applied to correct for static shift effects on the MT data. Dimensionality analysis was then used to classify the type of the subsurface structures. Phase Tensor analysis, one of the dimensionality tools, indicated low skew values at short periods (10^{2}–1s), suggesting predominantly 1D and 2D structures at shallow depths. In contrast, higher skew values observed at longer periods (10 s) pointed to the presence of complex 3D structures at greater depths. The regional structures are striking in a general trend of NE-SW as observed from the geo-electric strike estimation method. The resistivity models obtained from 2D and 3D inversion revealed three layers varying with depth. The upper near-surface resistive layer of > 100 Ωm, extending almost to 1 km above sea level. Beneath this layer is a conductive zone of about < 10 Ωm, which could be the possible reservoir seal. The third layer has a relatively high resistivity of > 80 Ωm, representing the possible reservoir zone ranging between 2.5 to 4 km.

CHAPTER ONE

INTRODUCTION

1.1 Background to the Study

Geothermal energy is vast in potential and naturally replenished, making it a reliable and renewable resource. It serves as a cost-effective alternative to fossil fuels, particularly for countries with abundant geothermal potential. In addition to its economic benefits, geothermal energy is environmentally friendly, producing no greenhouse gas emissions. Kenya is particularly rich in high-temperature geothermal resources, most of which remain underutilized. As a component of the East African Rift System's (EARS) eastern branch, the Kenyan Rift is linked to several resources. A developing divergent plate boundary known as the EARS was created when the Somali Plate started to split apart from the Nubian Plate. This tectonic movement created a rift extending northward to the Afar region in Ethiopia, where it intersects with the Arabian Plate, forming a Y-shaped rift system. The EARS is divided into two branches: the Eastern and Western branches. The Kenyan Rift falls within the Eastern branch, which is characterized by more intense tectonic and volcanic activity than the Western branch. This activity has led to the formation of large Quaternary shield volcanoes along the rift axis. In the central part of the Kenyan Rift, major Quaternary volcanoes include Barrier, Emuruangogolak, Silali, Paka, Korosi, Menengai, Eburru, Olkaria, Longonot, and Suswa. Many of these volcanic centers have been targeted for geothermal exploration and are at varying stages of development. Among them, the Olkaria volcanic complex is the most extensively studied and is in the most advanced stage of development (Ofwona *et al.,* 2006).

Geophysical methods have been extensively used to assess geothermal potential because they offer valuable insights into subsurface conditions without requiring drilling (Telford et al., 1990; Parasnis, 1986). The MT method is a geophysical technique widely used in geothermal exploration due to its ability to map subsurface resistivity structures. It is especially effective at identifying geothermal reservoirs and their overlying clay cap

rocks, which show strong resistivity contrasts. By measuring natural electric and magnetic fields, MT offers advantages such as flexibility, depth penetration, and cost-effectiveness (Cagniard, 1953; Campanya *et al.,* 2016). In the Olkaria geothermal field, MT is extensively used to explore structures from shallow depths to hundreds of kilometers. Before MT was introduced, the direct current (DC) resistivity method was commonly used in Olkaria (Omollo *et al.,* 2022).

In volcanic geothermal systems, which exceed 150°C and are driven by magmatic heat sources, resistivity is mainly influenced by hydrothermal alteration minerals and reservoir fluids. These fluids affect resistivity based on their salinity, temperature, saturation, porosity, and permeability, especially when forming well-connected networks within the rock (Munoz, 2014; Ussher *et al.,* 2000). The resistivity structure of a high-enthalpy system consists of four zones: a resistive surface layer (Zone 1), a highly conductive clay cap (Zone 2), an underlying resistive reservoir (Zone 3), and a deeper low-resistivity zone associated with the heat source or up-flow zone (Zone 4) as shown in Figure 1.1.

This study aims to investigate the geothermal potential in the eastern side of Olkaria Domes using the magnetotelluric method.

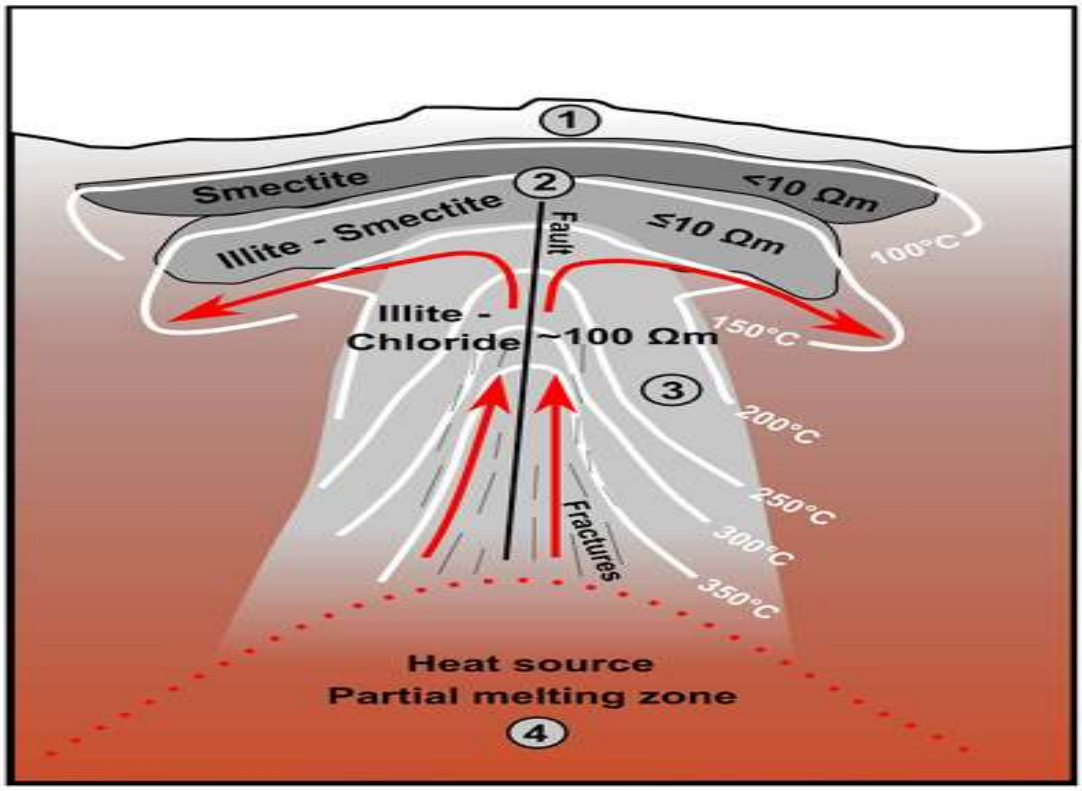

Figure 1.1: Sketch of the Conceptual Model of a High-Temperature Geothermal Reservoir

Source: (Johnston *et al*. 1992; Cumming. 2009).

1.2 The Study Area

The Great Olkaria Volcanic Complex (GOVC) is situated approximately 120 km northwest of Nairobi, and roughly 40km southwest of Naivasha (Figure 1.2). The resource area of the Olkaria geothermal field is estimated to be 204 km^2. Surface exploration in this field began in 1956, and the first exploration wells were drilled in 1970. Since then, wells have been drilled for different purposes, including exploration, production, makeup, step-out, re-injection, etc.

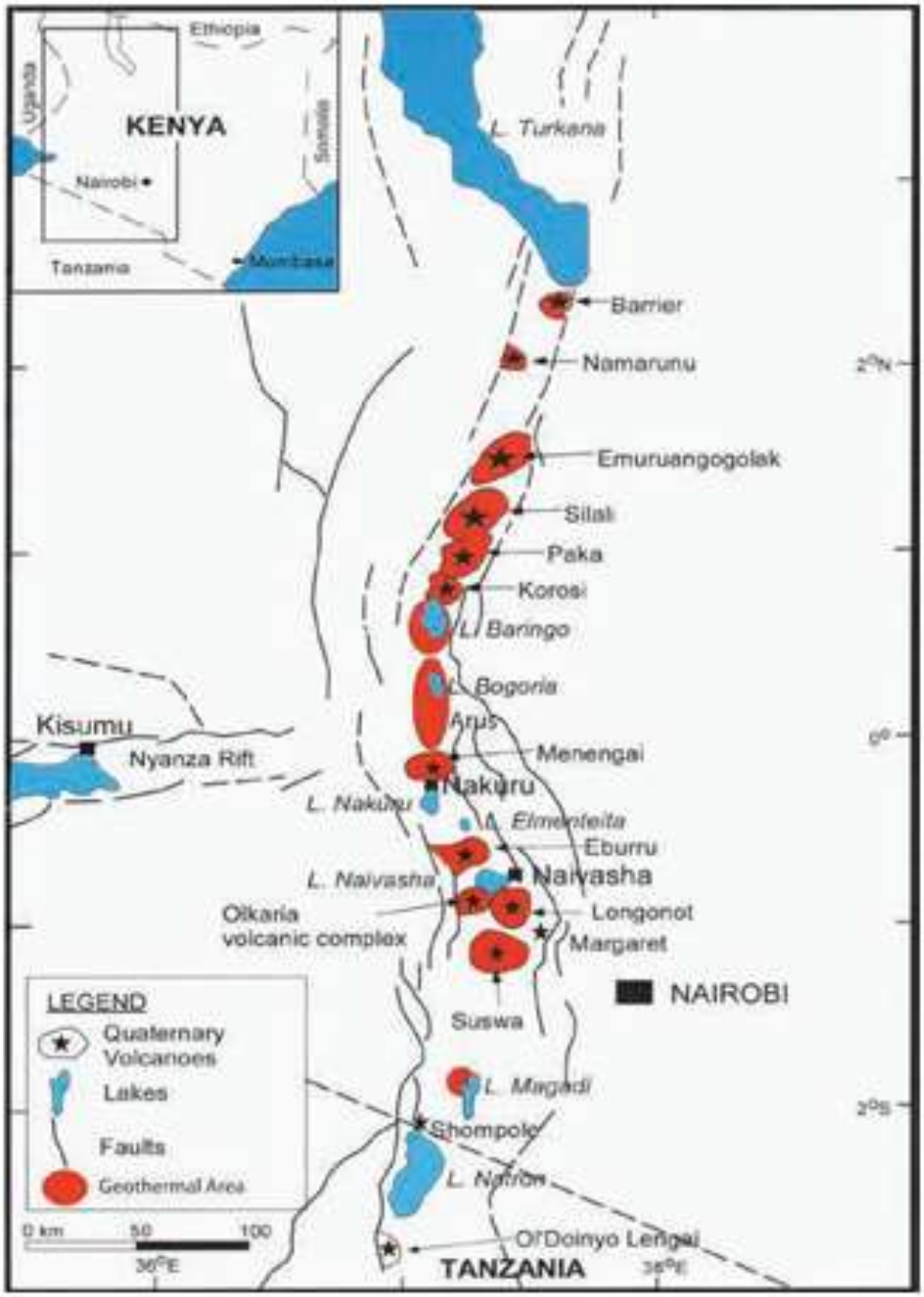

Figure 1.2: Potential Geothermal Prospects along the Kenyan Rift valley

Source: (Ofwona *et al.,* 2006).

To facilitate proper planning and development, the Olkaria geothermal field has been subdivided into seven distinct sub-fields: Olkaria East, Northeast, Central, Northwest, Southeast, Southwest, and Olkaria Domes, as illustrated in Figure 1.3, with Olkaria Hill serving as the central reference point. The Olkaria Domes geothermal field, situated in the southeastern part of the greater Olkaria area, is the most productive among these sub-fields. Consequently, this study focuses on the area east of the Domes field.

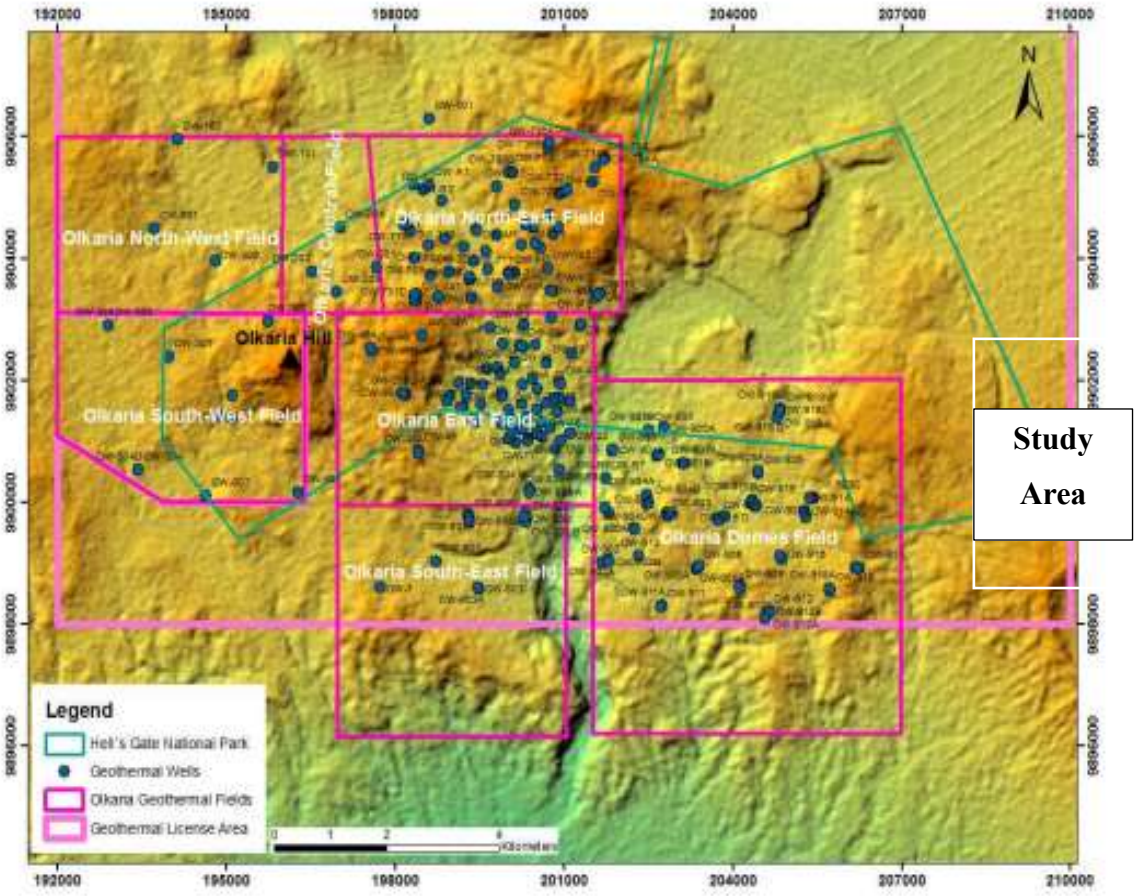

Figure 1.3: The Sub-Fields of the Olkaria Geothermal Field

Source: (Otieno and Kubai, 2013)

1.3 Geological Setting

The Olkaria geothermal field is a volcanic complex characterized by predominantly North-South trending normal faults and numerous rhyolitic volcanic domes (Axelsson *et al.,* 2017). It is a late Quaternary volcanic system situated within the central segment of the Kenya Rift, which forms part of the EARS. According to Chorowicz (1990), the rift system extends in a northwest-southeast direction, an important detail for understanding the structural orientation of the field. Olkaria exhibits a complex structural framework, with additional fault trends observed in the East-West and Northeast-Southwest directions. These structural features play a key role in the interpretation of the region's active geological and geothermal processes. Naylor (1972), suggested the existence of the ring structure, which is an alignment of rhyolite domes pattern in the field, and it precedes the north-south tectonic trending pattern in the Rift Valley zone. Hence, it prompted him to attribute it to the collapse of a large volcanic complex after it was devastated by an explosive eruption. Lava flows and pyroclastic deposits of Quaternary age and the ash fall from Mount Longonot overlie the surface geology of the Olkaria geothermal field (Figure 1.4) (Marshall *et al.,* 1998).

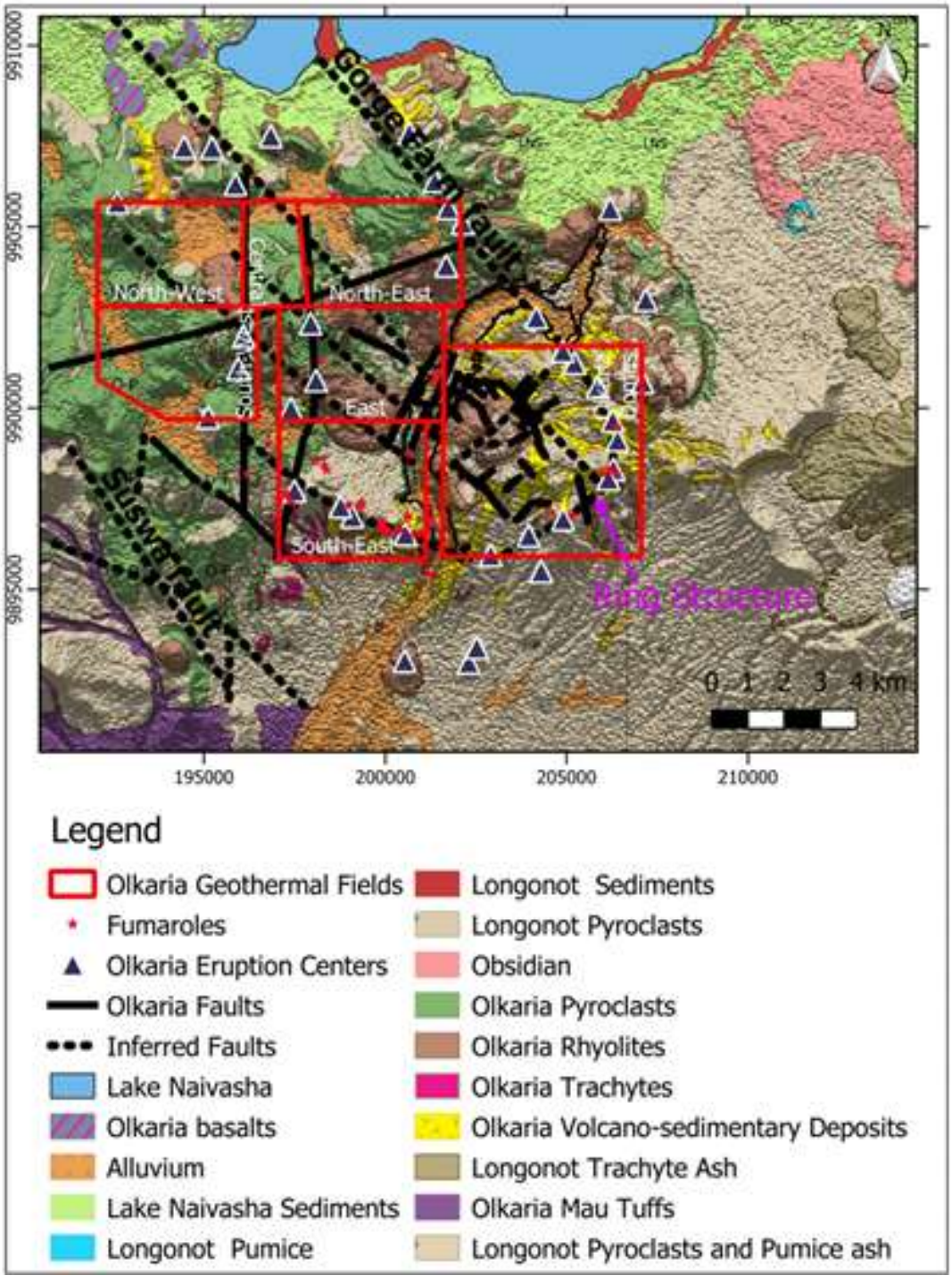

Figure 1.4: Structural and Surface Geological Map of Olkaria Geothermal Field

Source: (Modified by Omollo *et al.,* 2022).

The Ololbutot commenditic lava flow in the central Olkaria field is the most recent in Olkaria, dated by radio-carbon methods at about 180±50 BP (Clarke *et al.,* 1990). The surface geology of Olkaria is characterized by basaltic lava flows on the southwestern side of the field, along with comendite, pumice, and ash deposits. Subsurface rock types are primarily composed of tuff, trachyte, comendite, rhyolite, and basalts (Figure 1.4). Borehole analyses across the Olkaria field indicate that tuff and trachyte are the main reservoir rocks, with tuff dominating the western reservoir zones, while trachyte and basalt are predominantly found in the eastern reservoir areas (Omenda, 1998). The Olkaria geothermal field is traversed by fault structures that form a good pathway for meteoric water and magmatic fluids. The intersection of the faults enhances the subsurface permeability and provides good channels for permeating meteoric water to the shallow geothermal reservoirs. The recharge of the deeper geothermal reservoir in the Olkaria field is mainly through the major listric rift faults that are observed on the escarpments (Omenda, 1998). The permeability enhancement of the Olkaria geothermal field is attributed to the subsurface intersection of oblique faults and the north-south en-echelon faults that dissect the field, as observed from some wells' drilling logs.

Most pronounced structures within the field that influence geothermal reservoir conditions and fluid flow patterns trend in N-S, NW-SE, NNW-SSE, and ENE-WSW (Naylor, 1972). Structural features in the study area include lineaments and faults trending NNW-SSE, NE-SW, and NW-SE (Otieno, 2016). To the west of the Olkaria hills lies the Suswa lineament, which trends NW-SE along the western rift flank. This structure plunges into the Suswa caldera and reappears southeast of the volcano as a scarp. It also intersects the southwestern end of the Ol Njorowa Gorge, which crosses the field in a NE-SW direction. The Gorge Farm fault (NW-SE) and Olkaria fault (ENE-WSW) are believed to be linked to the formation of the rift and are among the oldest faults in the area. In contrast, faults trending N-S, NE-SW, and NNE-SSW are thought to be related to more recent tectonic activity (Omenda, 1998) and the proposed caldera collapse.

1.4 Statement of the Problem

Olkaria domes geothermal field is currently under development, with electricity being produced from two power plants and several wellhead generation units. However, the region to the east of the Domes remains largely unexplored in terms of geothermal resource assessment and production. Some preliminary geoscientific investigations were conducted in this area, utilizing a combination of one-dimensional Magnetotelluric (MT) and Transient Electromagnetic (TEM) methods to characterize the resistivity structure. This led to the drilling of an exploration well (OW-922), which unfortunately failed to sustain discharge during testing. As a result, it is evident that there is a need for a more detailed investigation to assess the presence of geothermal resources and enhance understanding of the subsurface system. To achieve this, 2D and 3D MT inversion models will be developed to map the resistivity structure in greater detail, thereby evaluating the geothermal potential of the survey area.

1.5 Justification of the Research

Since MT utilizes naturally occurring electromagnetic (EM) waves as its source of energy, it can investigate subsurface structures from shallow depths to significant depths. In this study, both 2D and 3D MT models were developed to gain a more comprehensive understanding of the resistivity distribution in the area. The findings will help characterize the subsurface resistivity structures and define the boundaries of the geothermal reservoir, providing valuable information for potential power generation. Estimating the size of the geothermal reservoir will support the expansion of the country's geothermal power capacity, thereby accelerating progress toward United Nations Sustainable Development Goals (SDGs) 7 and 8 on affordable and clean energy, and decent work and economic growth.

1.6 Objectives

1.6.1 General Objective

To investigate the geothermal potential in the eastern side of the Olkaria Domes using the magnetotelluric method.

1.6.2 Specific Objectives

1. To determine the presence and dimensions of the underlying structures by conducting dimensionality analysis of magnetotelluric data.
2. To develop 2D and 3D magnetotelluric models to characterize the subsurface structures on the eastern side of the Olkaria Domes geothermal prospect.
3. To estimate the extent of the geothermal reservoir in the study area.

CHAPTER TWO

LITERATURE REVIEW

2.1 Previous Studies

Hersir *et al*. (1990) detected a very low resistivity layer at 7.5 km depth in the Nesjavellir area, 3 km north of Mt. Hengill, which was interpreted as partial melt. Oskooi *et al*. (2005) also detected a shallow resistivity structure at ∼5 km depth south-west of Mt. Hengill, at the location of the fissure swarm, and interpreted it as either partial melt or a porous region with hot ionized fluids located on top of a magmatic heat source. Magmatic intrusions could act as a heat source for the geothermal system, although there is no seismic data to confirm the presence of magma at these locations.

Newman *et al*. (2008) conducted a study in the Coso geothermal field, USA using the MT method. The data was fully inverted to a three-dimensional (3D) resistivity model. This model shows the controlling geological structures possibly influencing well production at Coso and correlations with mapped surface features such as faults and the regional geoelectric strike. The 3D model also illustrates the refinement in positioning of resistivity contacts when compared to isolated 2D inversion transects.

The resistivity cross-sections from 1D joint inversion of MT and TEM data interpreted by Fantaye (2010) show three major resistivity structures. The high-resistivity uppermost layers of resistivity >70 Ωm are interpreted as unaltered basaltic dry lavas and hyaloclastites. The conductive cap (<10 Ωm) is associated with a smectite-zeolite or mixed-layered clay zone followed by resistive layers, corresponding to the chlorite-epidote zone. Generally, a good correlation is found between the subsurface resistivity structure and alteration mineralogy of the Krýsuvík high-temperature area.

Cumming and Mackie (2010) noted that MT is widely applied in geothermal exploration to guide well targeting and evaluate resource potential, as it effectively detects the low-resistivity, low-permeability smectite clay cap common to many geothermal reservoirs.

Gerard *et al*. (2018) presented electrical resistivity models obtained from the inversion of MT data along a regional 2D profile across the Eger Rift in the West Bohemia/Vogt land region. The dimensionality and directionality analysis of the data revealed a geo-electrical strike direction dominated by the Eger Graben and the profile perpendicular to it was considered for 2D inversion. Finite differences and finite elements inversion codes were used to generate electrical resistivity models, which show a consistent image of conductive and resistive features.

Further, the interpretation of MT and TEM data by Marwan *et al. (*2019) shows the low resistivity layer occurring up to a thickness of 1000 m according to both the TEM and MT data from the Seulawah Agam geothermal system interpreted as being composed of cap rock. The layer below the cap rock is likely to be a reservoir zone. The permeable pathway that is interpreted as the path of the manifestation fluid is also clearly seen in the MT model although it is not seen in the TEM model. The deep conductors below 2000 m b.s.l. could be the heat source for the Seulawah Agam geothermal system, which is located directly under Mount Seulawah Agam and extends to the Northwest side of the research area.

Arthur (2017) on MT data inversion results indicated a typical geothermal system in Korosi – Chepchuk geothermal prospect. The results further infer the possibility of the existence of two geothermal reservoirs within the prospect. The reservoir depth is estimated to be at sea level and a close correlation between major surface structures, fumaroles, and the 3D model is observed.

Maithya and Fujimitsu (2019) analyzed magnetotelluric (MT) data from the Eburru geothermal field in Kenya using both 2D and 3D inversion models. Their study showed that the two approaches yielded comparable results, identifying a low-resistivity layer (<10 Ωm) interpreted as a clay cap, with an underlying higher-resistivity zone interpreted as the geothermal reservoir located directly beneath the cap.

In recent years, joint 1D inversion has been the primary method used for data analysis and interpretation in the Olkaria field (Lichoro, 2010; Mwangi, 2018). This approach identified zones of both extremely low and high resistivity within the study area. However, earlier applications of the MT method offered limited lateral resolution of geological structures. As a result, the finer details and geometry of some subsurface features were not fully captured. To address these limitations, the use of 2D and 3D inversion techniques became essential for generating a more precise and comprehensive image of the subsurface.

Omollo *et al.,* (2022), in their interpretation of MT data inversion in Olkaria Domes, acknowledged that the 2D and 3D inversion of MT data revealed three layers varying with depth. The upper near-surface conductive layer of < 10 Ωm, extending almost to 1200 m above sea level, is considered the reservoir seal; below this is a resistive zone of about > 90 Ωm, representing the possible reservoir zone at about 2.5 to 4 km. The third layer at a depth of 5.5 to 8 km of the model with a moderate conductivity of < 20 Ωm, which is assumed to be the heat source, possibly consists of a partial melt facilitating a circulation zone (< 30 Ωm) of an upwelling hydrated magmatic fluid.

Munyiri (2016), in a structural mapping study of the Olkaria Domes geothermal field, noted that the eastern part of the Domes field remains largely underexplored. The region has limited geophysical data and only a single well has been drilled. As a result, further interdisciplinary scientific investigations are necessary to better assess and understand the area's geothermal potential.

2.2 Theoretical Background

2.2.1 The Theory of Magnetotelluric (MT) Method

MT is a passive method which uses the naturally occurring electromagnetic fields caused by the interactions between the solar wind and the magnetosphere and lightning discharges from the equatorial regions (Chave and Jones, 2012). The method is applied to image the subsurface resistivity structures of the study area since it relies on the natural

electromagnetic fields as its energy source. When primary electromagnetic fields reach the Earth's surface, they are both reflected and transmitted into the subsurface. As the Earth behaves like a conductor, it induces electric fields known as telluric currents which in turn generate secondary magnetic fields. These fields can penetrate from depths of less than a hundred meters to several hundred kilometers (Chave and Jones, 2012). MT is extensively used in geothermal exploration to map electrically conductive clay caps that overlay geothermal reservoirs and to identify shallow magmatic heat sources. Such applications have been demonstrated in regions like the Ethiopian Rift within the East African Rift System (Didana *et al*., 2015; Samrock et al., 2021), the Kirishima volcano on Kyushu Island, Japan (Aizawa et al., 2014), and the southeastern Tibetan Plateau (Ye *et al*., 2018).

The behavior and propagation of electromagnetic fields at any frequency is concisely summarized by Maxwell's equations. Maxwell's equations are expressed below in terms of B and E:

$$\nabla \times \mathrm{B} = \mu\sigma\mathrm{E} + \mu\varepsilon\frac{\partial \mathrm{E}}{\partial \mathrm{t}} \qquad \text{(Ampere's Law)} \qquad 2.1$$

$$\nabla \times \mathrm{E} = -\frac{\partial \mathrm{B}}{\partial \mathrm{t}} \qquad \text{(Faraday's Law of Induction)} \qquad 2.2$$

$$\nabla \cdot \mathrm{B} = 0 \qquad \text{(Gauss's Law for Magnetism)} \qquad 2.3$$

$$\nabla \cdot E = \frac{\eta}{\varepsilon} \qquad \text{(Gauss's Law)} \qquad 2.4$$

Where E is the electric field (Vm^{-1}), B is magnetic flux density (T), and η is the electric charge density owing to free charges (Cm^{-3}).

This is the modified form of Maxwell's equations in a conductive media and shows the coupling between the magnetic and electric fields.

Ampere's Law (Equation (2.1)) describes the magnetic field, which depends on the electrical current density of free charges and the time variation of the displacement current. Faraday's Law of Induction (Equation (2.2)) states that time variations in the magnetic field induce electric field flowing in a closed loop. Gauss's Law for Magnetism (Equation (2.3)) states that no free magnetic charges exist (i.e., magnetic monopoles). Gauss's Law (Equation (2.4)) states that electric charges act as sources for electric fields.

MT traces its origins to the foundational work of Tikhonov (1950) and Cagniard (1953), who laid the theoretical groundwork for the method. Over the past five decades, advancements in theoretical development, instrumentation, and data interpretation have significantly enhanced MT, establishing it as a robust geophysical tool for imaging diverse geological structures. A detailed historical overview is provided by Dupis (1997). The method utilizes natural electromagnetic signals: low-frequency components originate from ionospheric and magnetospheric currents driven by solar wind interactions with Earth's magnetic field, while high-frequency signals (above 1 Hz) primarily result from equatorial thunderstorms and propagate as guided waves between the Earth and the ionosphere, as illustrated in Figure 2.1. By recording temporal variations in surface electric and magnetic fields, MT enables the determination of subsurface resistivity structures (Hersir and Árnason, 2015).

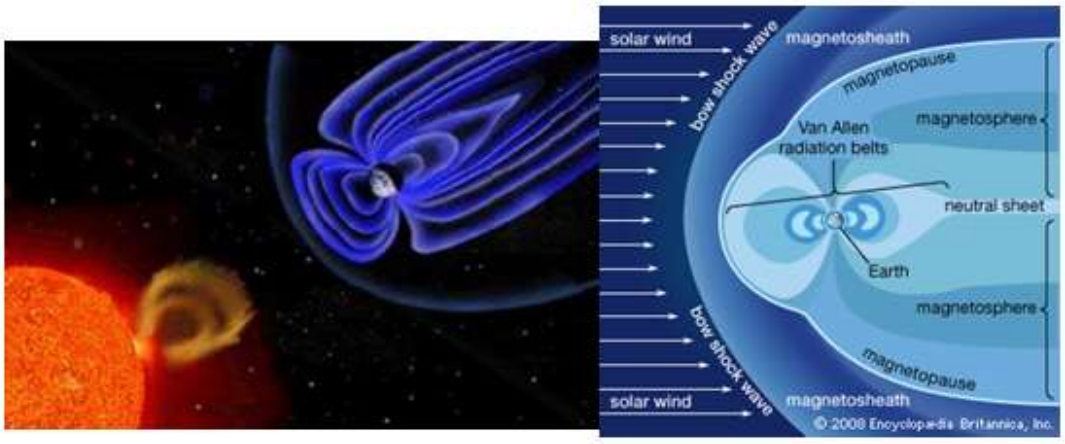

Figure 2.1: Interaction of Solar Wind with the Magnetosphere

Source: (Hersir and Árnason 2015).

MT data collected at different frequencies enables the differentiation of spatial variations in resistivity both vertically and laterally. The penetration of the electromagnetic field, which exponentially decays, is determined by the frequency and resistivity of the subsurface medium. Higher frequencies are more effective in mapping the resistivity distribution in the near-surface, while lower frequencies can penetrate deeper and provide information on subsurface structures.

For homogeneous earth, the resistivity, ρ, is given as:

$$\rho = \frac{1}{\omega \mu_o} |Z|^2 \qquad 2.5$$

Where ω is the angular frequency of the signal, $\mu_0 = 4\pi \times 10^{-7}\ H/m$ is the magnetic permeability of free space, and $Z = E_x/H_y$.

According to Cagniard (1953), equation 2.5 can be expressed as,

$$\rho = 0.2T\frac{|E_x|^2}{|H_y|^2} \quad 2.6$$

Where, T = Period in s, E = Horizontal electric field (mv/km), and H = Orthogonal horizontal magnetic field in gamma.

Equation 2.7 defines apparent resistivity in the case of heterogeneous resistivity

$$\rho_{a=}0.2T|Z|^2 = \frac{|E_x|^2}{|H_y|^2} \quad 2.7$$

Where Z = Impedance at the surface.

In MT, the depth of investigation depends on the subsurface resistivity and the frequency (or its inverse, the period) of the electromagnetic signals. The penetration depth can be approximately estimated using the concept of skin depth. The skin depth δ (m) at which the electromagnetic field amplitude is reduced to e^{-1} of its original value at the surface is given as:

$$\delta = \sqrt{\frac{2}{\omega\mu_0\sigma}} \approx 0.5\sqrt{\rho_a T} \quad 2.8$$

2.2.2 The Galvanic Distortion Phenomenon

Distortion in MT refers to an effect caused by small, shallow local structures or variations in the Earth's subsurface. These features are significantly smaller than the main targets of interest and the depth to which the electromagnetic signals penetrate. When such structures are present, they create charge distributions and induced currents, leading to changes in the overall MT responses observed on a regional or local scale. If these small structures have similar dimensions as the depth of interest, they can be effectively represented and studied using a 3D modeling approach. Distortion in MT can be categorized as either inductive or galvanic. Inductive distortion is primarily caused by

current distributions and tends to have a relatively small magnitude (Berdichevsky and Dmitriev, 1976). Galvanic distortion in MT arises due to the presence of charge accumulations on the surface of shallow bodies. These accumulations lead to the generation of an anomalous electromagnetic field. The resulting anomalous magnetic field is typically of minor significance, while the anomalous electric field is comparable in magnitude to the regional electric field and does not vary with frequency (Bahr, 1988; Jiracek, 1990). Because of this behavior, galvanic distortion is often interpreted as the presence of an unusual electric field. Mathematically, the effect of this electric field on the transfer functions can be represented by a 2x2 real, frequency-independent, and non-dimensional matrix, C (Berdichevsky and Dmitriev, 1976).

$$C = \begin{pmatrix} C_1 & C_2 \\ C_3 & C_4 \end{pmatrix} \tag{2.9}$$

The elements of *C* rely on the geometry and position of the distorting body as well as on the resistivity contrast between the body and the surrounding medium (Jiracek, 1990).

2.2.3 MT Static Shift Problem

Static shift in MT is a phenomenon that occurs when there are contrasting conductivities in the local surface or near-surface environment, leading to changes in the magnitude and direction of the electric field. Static shifts typically arise when the dimension of anomalous bodies is much smaller than the skin depth. Most electrical methods that measure the electric field at the Earth's surface are prone to issues related to static shift. This arises from the accumulation of electric charges at resistivity boundaries, causing irregular behavior of the electric field near these zones. Static shift is caused by voltage and current distortion, which can introduce distortions in the measured voltage and current signals (Árnason *et al.,* 2010). The static shifted data is expressed by an unknown factor (shifted on a log scale) that scales the apparent resistivity, such that the apparent resistivity curves plot parallel to their real level. The shift is independent of frequency (Jones, 1988) and does not affect the phase curve. Failure to properly correct for static shift effects in MT

data can lead to inaccurate. In this study, we used the spatial median filter method to address the static shift problem.

2.2.4 Spatial Median Filter Method

This method evaluates each sounding by comparing it with others located within a defined radius over a specific period range. It calculates the median apparent resistivity for each polarization based on stations within that radius. If the difference between a sounding and the median exceeds a set tolerance, it is considered a static shift and is corrected by adjusting both components of the impedance for that polarization (Berdichevsky & Dmitriev, 2008).

2.3 Dimensionality Analysis

Dimensionality analysis is performed to assess the nature of the subsurface geo-electrical structures. This evaluation helps determine whether the observed data at a specific frequency reflects a 1D, 2D, or 3D structural framework. It also helps identify and quantify any distortions in the data and supports the determination of the geological strike direction. Overall, dimensionality analysis enhances the understanding of subsurface features and guides the selection of an appropriate MT modeling strategy (Marti *et al.,* 2010). The various dimensionality assessment tools used are described below.

2.3.1 Swift and Bahr skew

Skewness is a key parameter used in MT to evaluate the dimensionality of subsurface structures. The Swift skew method, developed by Swift in 1967, relies on the MT impedance tensor and is mainly based on the amplitude response tensor. This technique helps interpret the data by indicating whether the underlying geological formations can be approximated as 1D, 2D or 3D.

The Swift skew is defined as follows:

$$Swift\ skew = \frac{(z_{xx} + z_{yy})}{(z_{xy} - z_{yx})} \quad 2.10$$

A notable limitation of the Swift skew method is its susceptibility to distortions resulting from the interaction between regional 1D or 2D inductive responses and localized, small-scale conductive anomalies (Simpson and Bahr, 2005). To overcome this issue, Bahr (1991) introduced an alternative approach that utilizes skew values derived from the phases of the impedance tensor. Unlike amplitude-based methods, these phase-based skew values are not influenced by distortion effects from small-scale conductive features or other local disturbances. By focusing on phase information, this method offers a more robust and reliable analysis of subsurface dimensionality, even in distorted environments. The Bahr's phase-sensitive skew is given by

$$Bahr's\ skew = \frac{|[D_1 S_2] - [S_1 D_2]|^{1/2}}{|D_2|} \quad 2.11$$

Where, $S_1 = Z_{xx} + Z_{yy}$; $S_2 = Z_{xy} + Z_{yx}$, $D_1 = Z_{xx} - Z_{yy}$; $D_2 = Z_{xy} - Z_{yx}$

Generally, if skew values are > 0.3, then it implies that the MT data are 3D.

2.3.2 Phase Tensor

Phase tensor analysis is a crucial method for assessing the dimensionality of subsurface structures because it is not affected by galvanic distortions. It provides distortion-free phase information on a regional scale (Caldwell *et al.,* 2004; Moorkamp, 2007). The phase tensor is defined by:

$$\Phi = \mathrm{X}^{-1}\mathrm{Y} = \begin{bmatrix} Z_{xx} & Z_{xy} \\ Z_{yx} & Z_{yy} \end{bmatrix} \quad 2.12$$

Where X and Y are the real and imaginary parts of the impedance tensor (Z).

Caldwell *et al.,* (2004) introduced the "skew" parameter (β) to describe the inherent dimensionality of subsurface features based on the phase tensor which is visually represented as an ellipse (Figure 2.2). The ellipse's major axis (φmax) indicates the maximum phase, while the minor axis (φmin) represents the minimum phase. Evaluating the skew parameter (β) is vital for identifying the dominant dimensionality of subsurface structures. For 1D cases, the phase tensor ellipse approximates a circle because φmax and φmin are nearly equal, resulting in a skew (β) close to zero. In 2D structures, although φmax and φmin differ, a skew (β) of zero is necessary but not sufficient (Caldwell et al., 2004). When the ellipse's major axis rotates by an angle (β), known as the geoelectrical strike angle, it aligns either parallel or perpendicular to the regional strike direction. This alignment leads to a 90° ambiguity, corresponding to either the TE or TM mode.

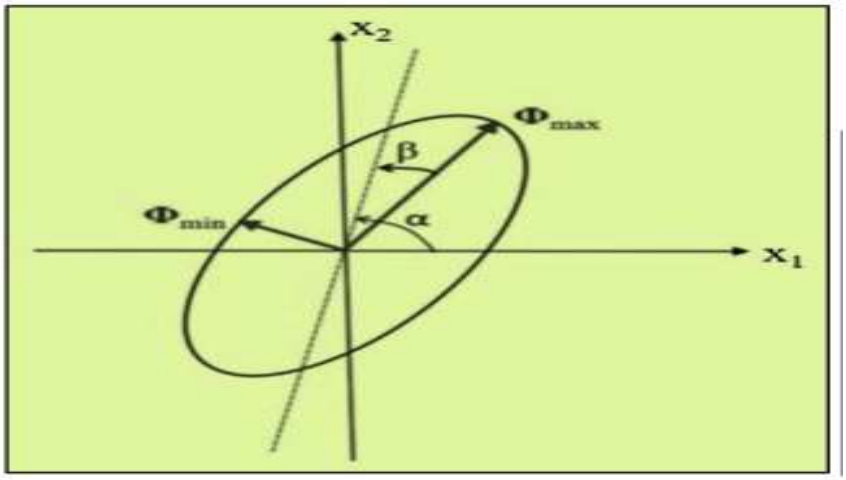

Figure 2.2: Elliptical Representation of the Phase Tensor

Source: (Caldwell *et al.,* 2004).

The skew angle (β) quantifies the degree of deviation from two-dimensionality. When the absolute value of β is less than 30° (|β| < 30), it indicates a "quasi-2D" structure, meaning the subsurface features largely exhibit two-dimensional characteristics. For a 3D structure, β is non-zero, signaling a distinct departure from two-dimensionality. In this case, the orientation of the major axis of the phase tensor ellipse is given by the angle (α-β),

reflecting the complex three-dimensional arrangement of the subsurface structures. At shorter periods, the phase tensors appear nearly circular along the profile, suggesting a 1D structure. However, as the period increases, the circles transform into ellipses, revealing asymmetry in the regional MT response caused by mid-crustal inhomogeneities. At lower frequencies, $|\beta|$ is greater or less than $5^{0,}$ indicating that the subsurface structure is 3D. The analysis method by Phase Tensor was applied in characterizing the dimensionality of local and regional subsurface structures because it is insusceptible to galvanic distortion.

2.4 Occam's and ModEM Inversion Codes

2.4.1 2D Inversion

In a 2D Earth model, the off-diagonal elements of the impedance tensor are categorized into two modes: transverse magnetic (TM), which is perpendicular to the strike direction, and transverse electric (TE), which is aligned parallel to the geo-electric strike direction. The dimensionality of the subsurface structures is indicated by the diagonal components of the impedance tensor. For an environment dominated by 2D structures, the presence of 3D structures affects the data and is treated as noise. The interpretation of TM mode in 2D is considered more accurate than TE mode in 3D structures, while TM mode is documented to respond well to both 2D and 3D conductive structures (Degroot-Hedlin and Constable, 1990). In this study, we used the Occam 2D inversion code (version 3.0), which was created by Scripps Institution of Oceanography based on Degroot-Hedlin and Constable (1990).

2.4.2 3D Inversion

The ModEM code created by Egbert and Kelbert (2012), Meqbel (2009), and Kelbert *et al.,* (2014) was used to analyse the MT data and generate a 3D resistivity model. Using the parallelised nonlinear conjugate gradient (NLCG), this algorithm solves the penalty function effect minimisation problem (Equation 2.13).

$$\mathrm{U}(\mathbf{m},\mathbf{d}) = \big(\mathbf{d}-\mathbf{F}(\mathbf{m})\big)^{T}\mathbf{C}_{\mathbf{d}}^{-1}\big(\mathbf{d}-\mathbf{F}(\mathbf{m})\big) + \lambda(\mathbf{m}-\mathbf{m}_0)^{T}\mathbf{C}_{\mathbf{m}}^{-1}(\mathbf{m}-\mathbf{m}_0) \qquad 2.13$$

The difference $\mathbf{d}-\mathbf{F}(\mathbf{m})$ from Equation 2.13 is the nonconformity of the measured data, $\mathbf{d}$ and the forward mapping response $\mathbf{F}(\mathbf{m})$ of a conductivity model m, where m_0 is a priori guess model parameter. C_d and C_m are the data errors covariance matrix and the model covariance matrix (regularization matrix), respectively. λ is a trade-off parameter between data misfit and model structure.

CHAPTER THREE

MATERIALS AND METHODS

3.1 Materials

The instrumentation used consisted of a 5-channel MT data acquisition system (MTU-5A) from Phoenix Geophysics, a Global Positioning System (GPS), a 12 V battery, flash memory for data recording, and telluric and magnetic cables.

3.2 Method

3.2.1 MT Data Acquisition

The data used in this study was acquired by KenGen staff using a 5-channel MT data acquisition system (MTU-5A) from Phoenix Geophysics in 2023. The terrain determined the spacing between stations which varied from 300 to 500 meters. The horizontal orthogonal magnetic field, Hx (usually aligned in the magnetic North-South direction), Hy (perpendicular to Hx), and the vertical magnetic field Hz were measured by magnetic coils. The distance between each pair of electrodes (Ex and Ey) was 60 m. Both electrodes were in contact with the ground and connected to the MTU-5 (data logger) that stores the measured signal (Figure 3.1). The non-polarizable electrodes consisted of sodium chloride solution in a ceramic container designed to ensure good contact between the outside wires and the soil. A GPS unit was utilised to give geographical coordinates and a continuous time signal, which are required for time series recording. The electromagnetic fields were digitally captured over time using an acquisition unit, with the time series data stored on a memory card. At each site, the horizontal electric field components and all magnetic field components were recorded continuously for about 18 hours. The measurement takes longer at a site to obtain strong enough signals, particularly at night when background noise is lower, resulting in a greater proportion of high-quality data and measuring a wide range of frequencies.

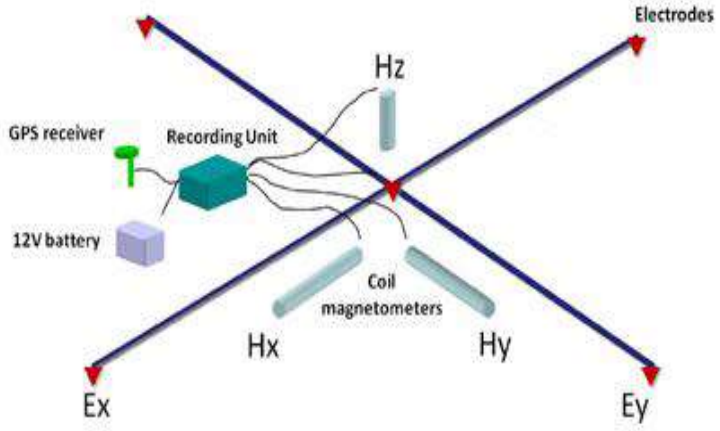

Figure 3.1: A Typical MT Field Set-Up

Source: (Hersir and Árnason, 2015)

3.2.2 MT Data Processing

The time-series data obtained from the MTU-5 units were processed using the SSMT2000 software developed by the equipment manufacturer, Phoenix Geophysics of Canada (Phoenix Geophysics, 2005). First, the parameter file was modified to reflect the data acquisition configuration, and the resulting time-series data was Fourier transformed to the frequency domain using the Cascade decimation method. The Robust processing approach was used to calculate band-averaged cross and auto powers from the Fourier transform band. The cross-powers were then graphically edited using the MT-Editor application. MT-Editor is a Windows-based program that takes input files created by SSMT2000, hence removing the noisy data points and evaluating "smooth curves for both phase and apparent resistivity. The final cross- and auto-powers, as well as all relevant MT parameters calculated from them, were stored in industry-standard file format in the form of Electronic Data Interchange (EDI) files. The EDI file was ready for plotting the resistivity and phase, and for making 2D and 3D inversions.

3.3 MT Data Analysis

3.3.1 2D Inversion

Parallel profiles for 2D inversion were selected from west to east to cut across the geological structures. The two analysed profiles (Figure 3.2) were inverted using a rectangular 50 m wide mesh of 70 layers, beginning with a layer thickness of 20 m and increasing logarithmically with depth. All inversions were treated to an initial model of 50 Ωm homogeneous half-space. To achieve model inversion, a maximum of 100 iterations was employed, with a target r.m.s of 0.5 and a maximum of 80 frequencies ranging from 0.011 to 320 Hz. The two models showed a minimum r.m.s misfit of 0.97 and 1.47 for profiles 1 and 2, respectively. A strike estimation of 45^0 was taken as the regional strike direction.

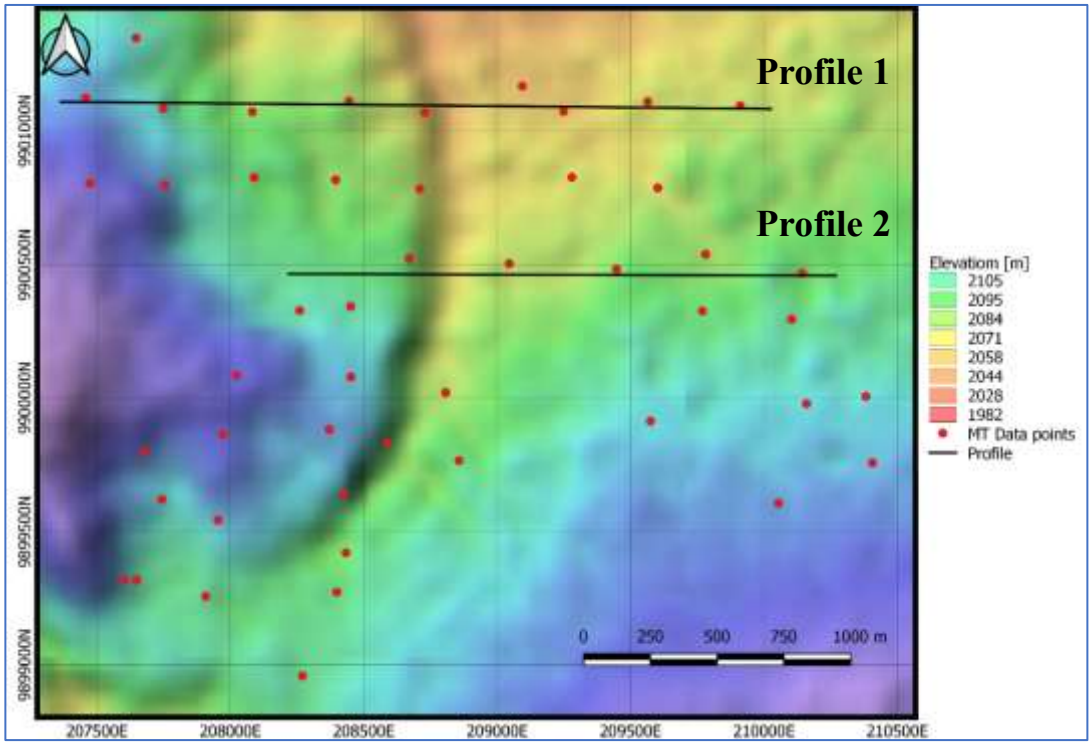

Figure 3.2: MT Data Station Distribution and Profiles

3.3.2 3D Inversion

50 MT soundings were used for 3D inversion. The inversion used a starting model of 50 Ωm. The user must assign the starting model; otherwise, it will be used by default. 200 cell dimensions in x and y axes were used, while in the Z direction, 48 layers were assigned with the initial layer thickness of 10 m, subjected to an increasing factor of 1.1, and padded with five cells in both the X and Y directions. The procedure produced a 3D subsurface structural geometrical model of the eastern side of Olkaria Domes with a depth of 10 km and 25×28×48 cells in the X, Y, and Z axes, as shown in Figure 3.3.

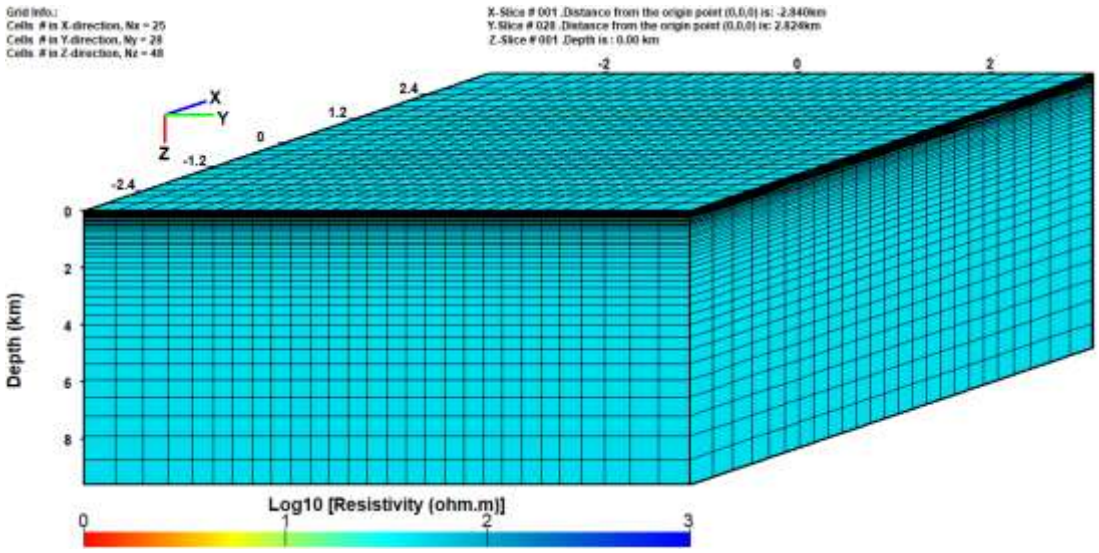

Figure 3.3: Grid Model of the Study Area

CHAPTER FOUR

RESULTS AND DISCUSSION

4.1 Static Shift Correction

Figure 4.1 shows the apparent resistivity and phase curves for stations dmt702 and dmt706, both before and after the removal of distortion and static shift. To correct the static shift issue during 2D inversion, a spatial median filter with a 3 km diameter was applied to each station, leading to a notable separation in the apparent resistivity curves at high frequencies.

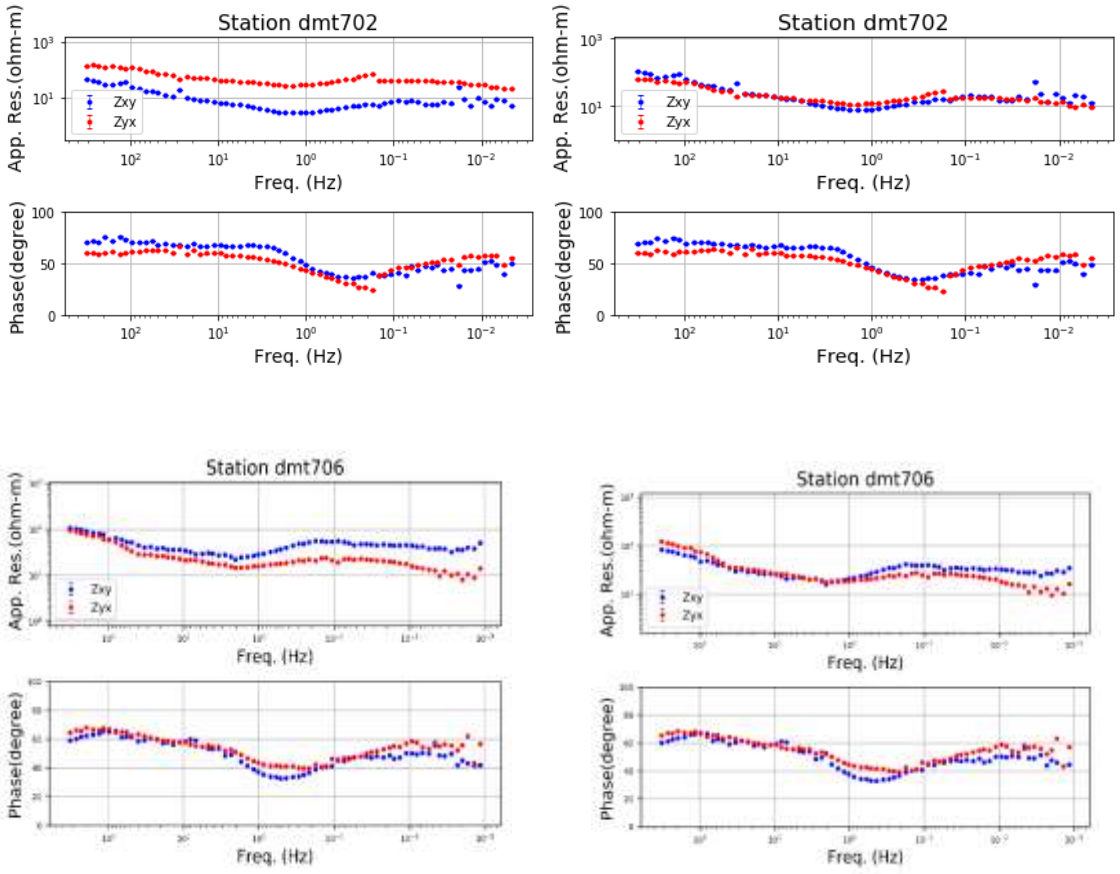

Figure 4.1: MT Data Curves Before and After Static Shift and Distortion Removal

4.2 Data Imaging

MT sounding curves give results for the anticipated structures following inversion. MT-sounding curves for transverse magnetic and transverse electric modes gathered from 50 locations on the eastern side of the Olkaria domes are shown in Figure 4.2. The TE mode is shown by red dots, and the TM mode is shown by blue dots. Both modes' apparent resistivity exhibits high values for short periods (< 0.01s) and decreases as the period increases to less than 1 second. It then progressively rises to a comparatively greater value of 10 seconds before dropping to a period of 100 seconds. High frequencies reflect responses from shallow depth structures, and low frequencies reflect responses from structures at deeper zones.

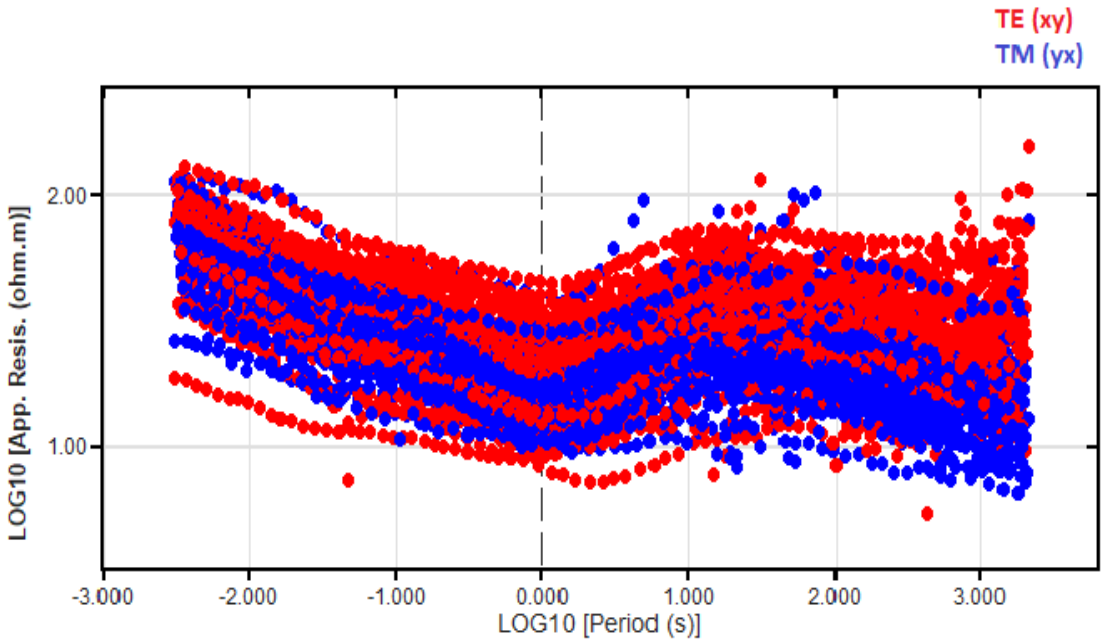

Figure 4.2: Apparent Resistivity Curves from 50 Stations of the Eastern Side of Olkaria Domes

4.3 Phase Tensor in Dimensionality Analysis

Dimensionality analysis of the eastern section of the Olkaria Domes was carried out using phase tensor data across various frequencies, with selected results presented in Figures 4.3 to 4.6. At higher frequencies (above 1 Hz), corresponding to shorter periods (10^{-2}–1 s), the data primarily exhibit 1D to 2D characteristics of the near-surface layers. Localized structural effects are indicated by yellow shading and low skew angles, particularly evident in the shallow subsurface as illustrated in Figures 4.3 to 4.5. In contrast, at lower frequencies (longer periods around 10 seconds), some stations display more complex responses, characterized by blue and red coloring in Figure 4.6, suggesting the presence of 3D resistivity structures.

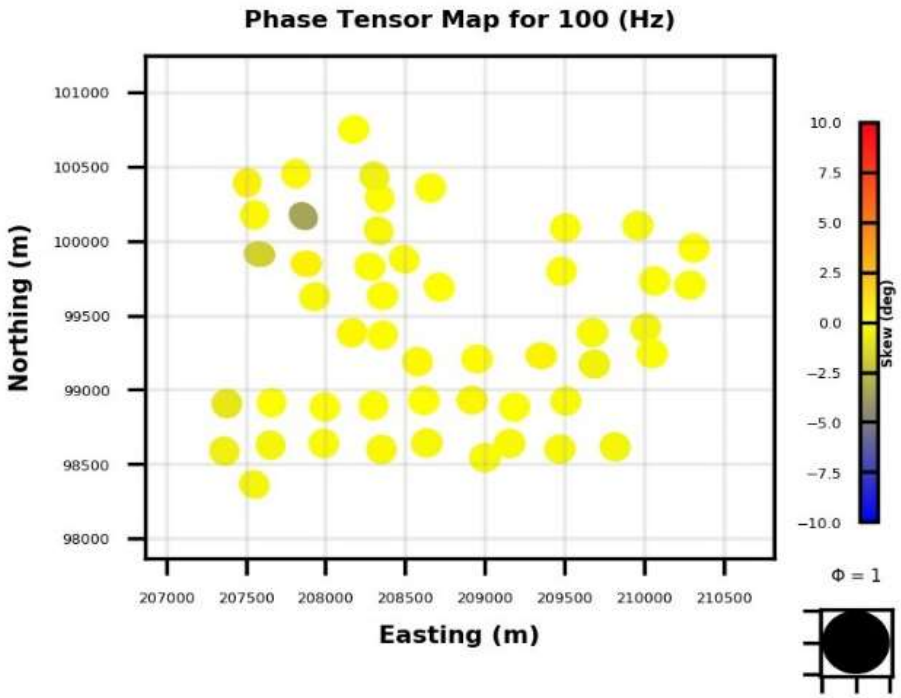

Figure 4.3: Phase Tensor Maps at 100 Hz

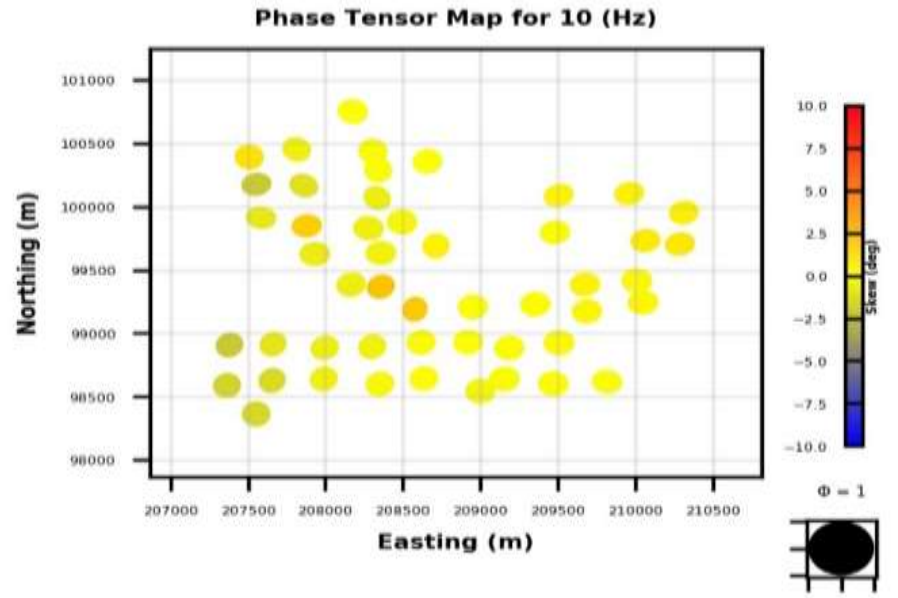

Figure 4.4: Phase Tensor maps at 10 Hz

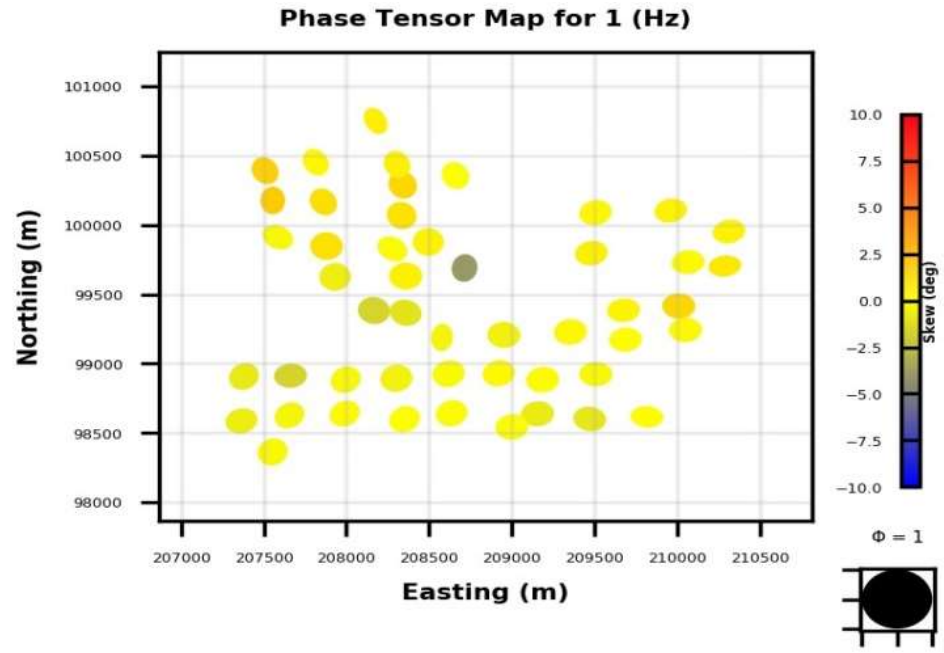

Figure 4.5: Phase Tensor Maps at 1 Hz

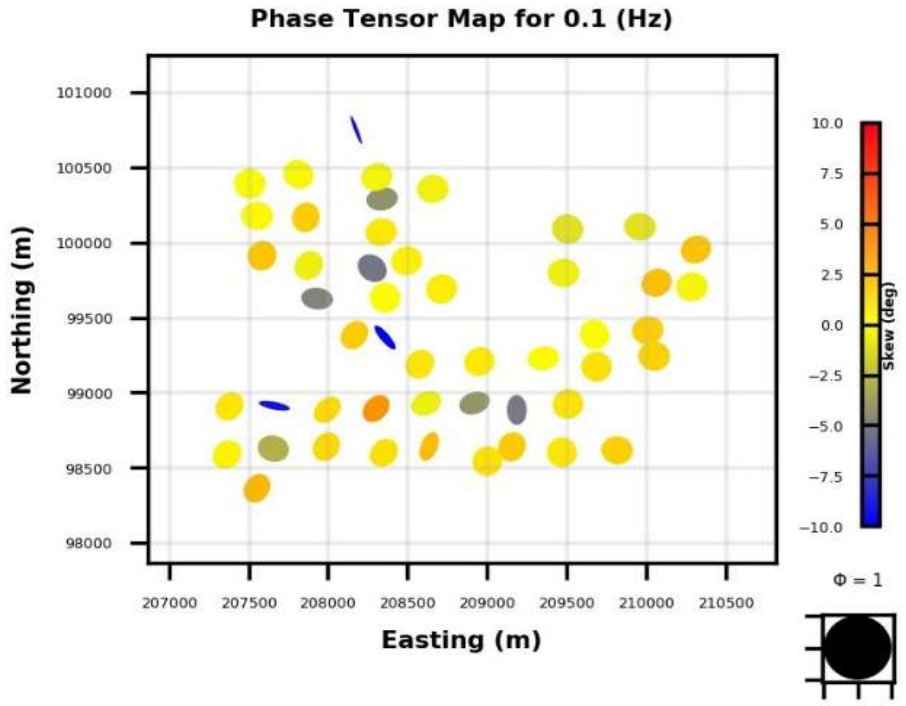

Figure 4.6: Phase Tensor Maps at 0.1 Hz

4.4 Strike Angle Estimation

When dimensionality analysis indicates the presence of 2D structures, it is essential to determine the geo-electric strike direction. This was established using the rose diagram strike estimation method. The strike angle estimates at short periods (<1 s) are scattered, due to contributions from shallow local structures. At periods (in the period band 1 – 10 s), there is a consistent strike direction of 45 degrees for the dataset. As shown in Figure 4.7, the geo-electric strike is approximately 45° at periods of 1 to 10 seconds, aligning with the NE-SW regional structural trend of the Olkaria field.

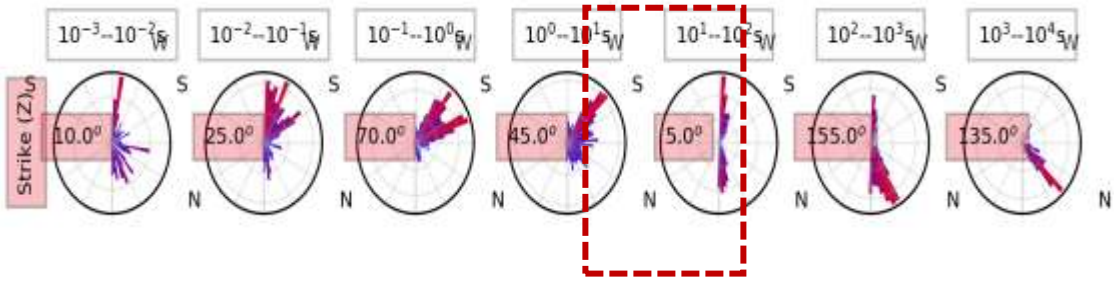

Figure 4.7: Rose Diagrams of Strike Estimates for the East of the Domes Field Data Set

4.5 MT Data Inversion

4.5.1 2D Inversion results

The inversion models extracted from the TE and TM modes of the MT data show consistent features along the profile. As illustrated in Figures 4.8 and 4.9, the pseudo-section plots for both measured and predicted responses indicate a strong correlation. Notably, the TM mode exhibits a slightly better fit than the TE mode, with smaller residuals observed for Profile 1.

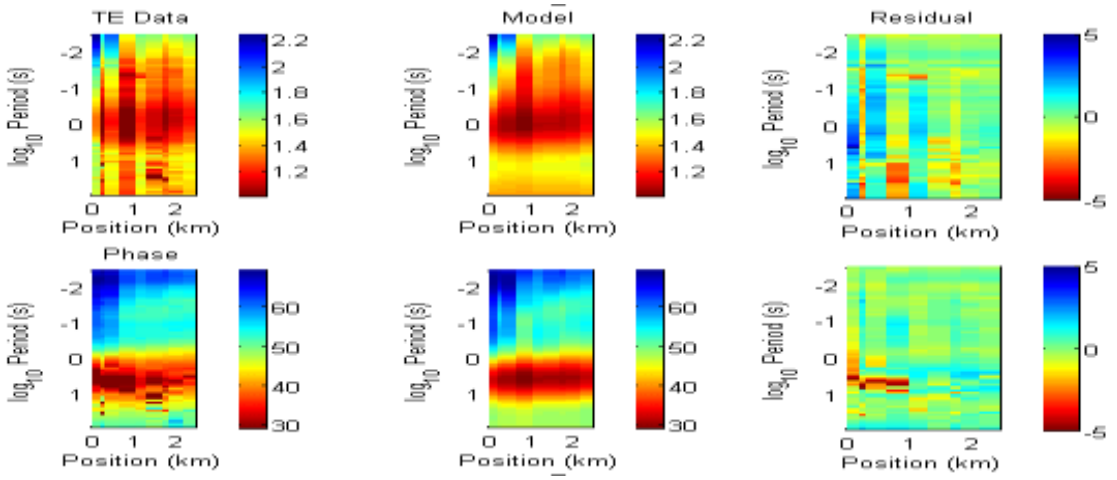

Figure 4.8: Pseudo Sections of Observed and Calculated Apparent Resistivity and Phase for TE Mode for Profile 1

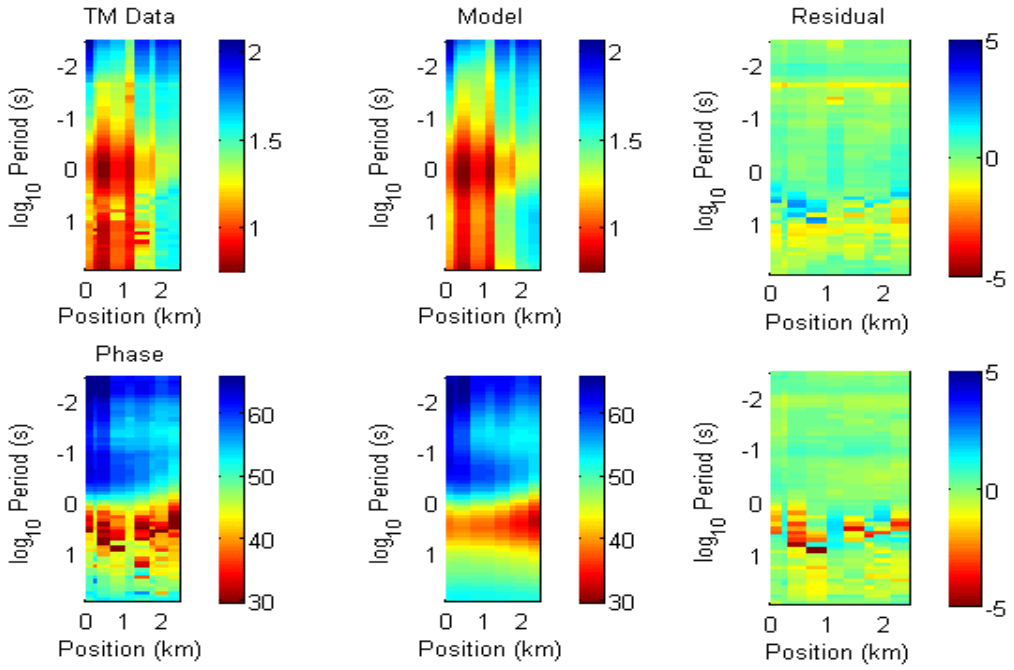

Figure 4.9: Pseudo Sections of Observed and Calculated Apparent Resistivity and Phase for TM Mode for Profile 1

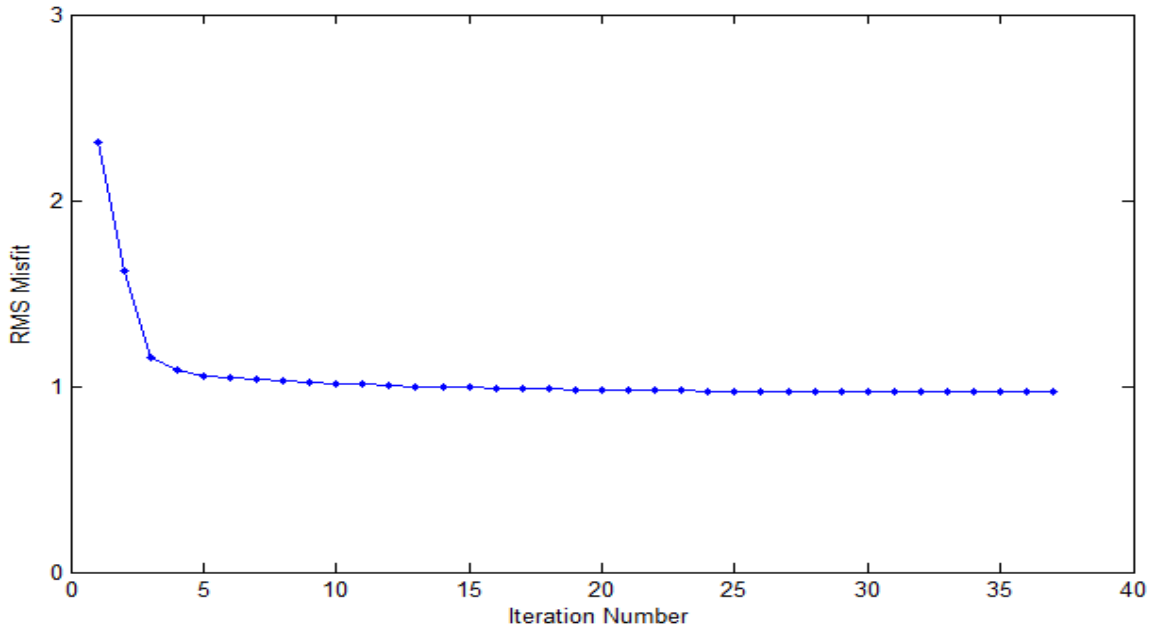

Figure 4.10: Graphic of rms Misfit versus Iteration Number of Profile 1

The rms misfit for profile 1 inversion is as shown in Figure 4.10. The RMS value for profile 1 converges towards a minimum value of 0.97, after 37 iterations. A smoothly decreasing RMS misfit is a sign of a stable inversion.

Figures 4.11 and 4.12 show the resistivity models obtained from the two profiles. The results revealed distinct conductive channels and resistive anomalies resulting from 2D Occam inversion.

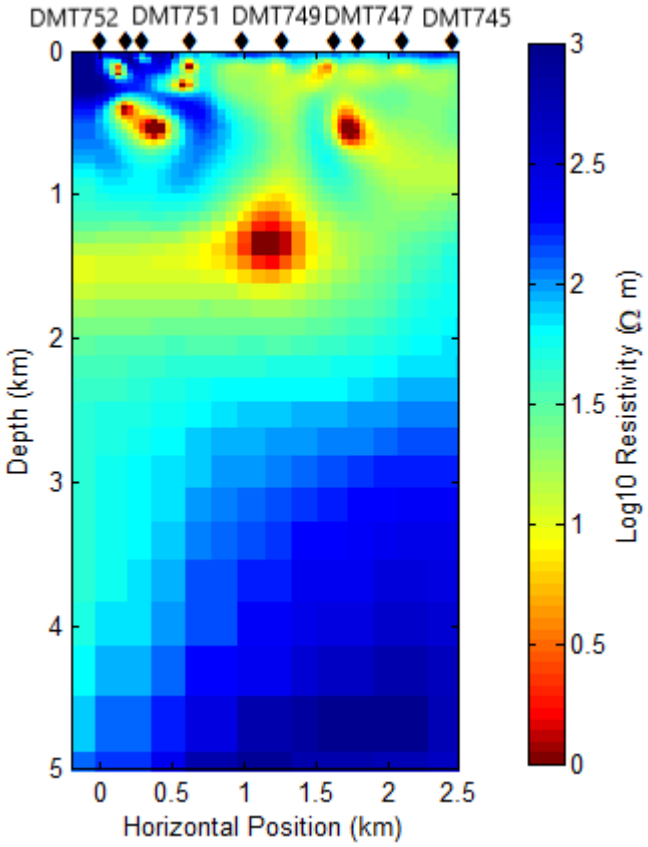

Figure 4.11: 2D Resistivity Models for Profile 1

Figure 4.11 presents a 2D resistivity model along Profile 1, which includes 10 MT soundings extending over a lateral distance of 2.5 km and reaching a depth of 5 km. The model reveals a highly resistive surface layer (>100 Ωm) extending across the entire profile, with an approximate thickness of 0.5 km. This layer likely corresponds to

unaltered surface formations. With increasing depth, resistivity significantly decreases to values below 10 Ωm, which may indicate zones of hydrothermal alteration associated with clay caps. Beneath this conductive layer, a moderately resistive zone (10–60 Ωm) appears at a depth of around 3.5 km, trending from east to southwest, and is interpreted as a possible extension of the geothermal reservoir.

Figure 4.12 shows the 2D model for profile 2, situated beneath profile 1. The model reveals a conductive zone (<10 Ωm) that appears to connect with the main conductive channel from profile 1, imaged at a depth of approximately 2 km. This conductive feature is flanked by two resistive structures that form a barrier-like configuration. A highly resistive anomaly (>100 Ωm) is observed at around 4 km depth, which is considered an extension of the features detected in profile 1, potentially representing the inflow of colder formations into the geothermal system.

In geothermal environments, clay cap layers are typically characterized by low resistivity values (≤10 Ωm) (Pellerin et al., 1996), while reservoir zones generally exhibit higher resistivity values ranging from 10 to 60 Ωm.

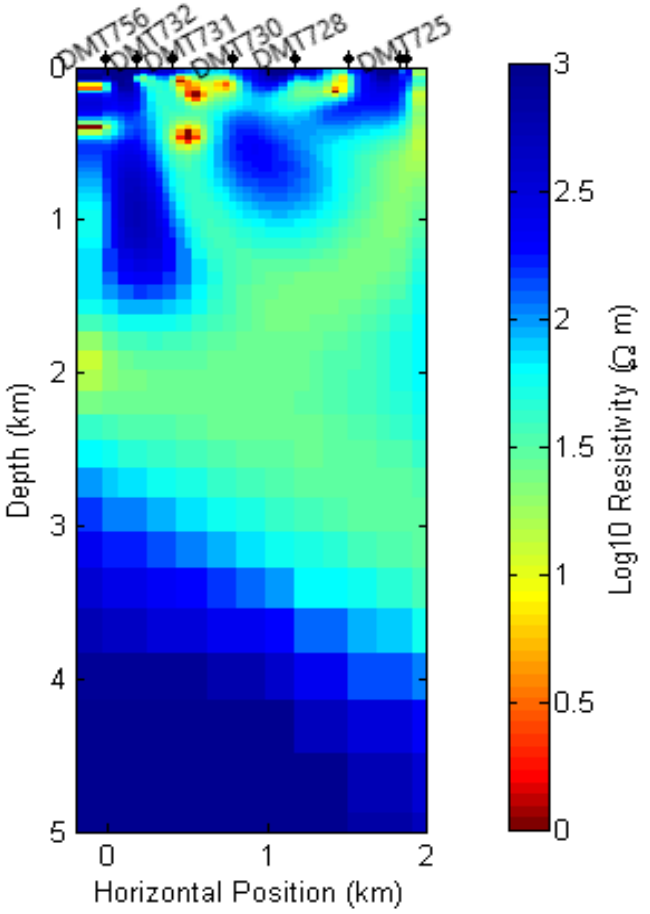

Figure 4.12: 2D Resistivity Models for Profile 2

4.5.2 3D Inversion Results

Data misfit is quantified as the difference between the observed MT data and the data predicted by the model during inversion. A smaller data misfit obtained indicates that the model approximated the observed data suggesting a more accurate and reliable representation of the subsurface resistivity structures as shown in Figures 4.13 and 4.14.

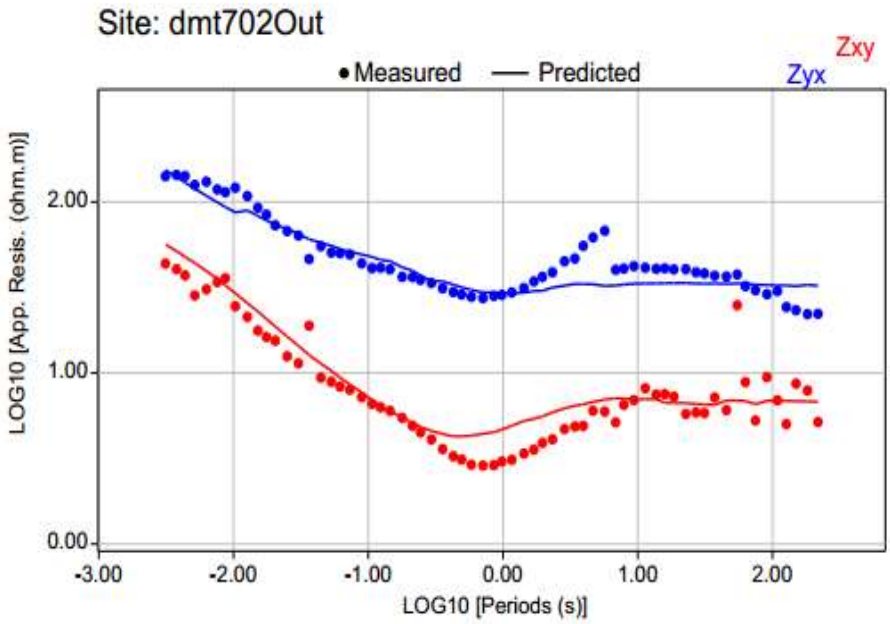

Figure 4.13: Data Misfit between the Measured and Predicted Apparent Resistivity Components for Station dmt702

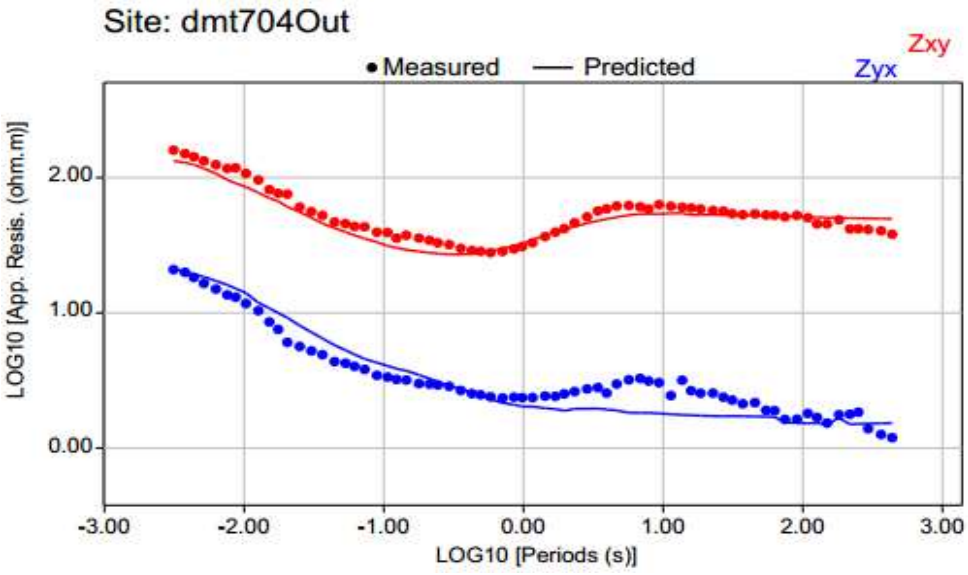

Figure 4.14: Data Misfit between the Measured and Predicted Apparent Resistivity Components for Station dmt704

The resistivity distribution model recovered from the 3D inversion using the ModEM program has three distinctive layers as illustrated in Figure 4.15. The uppermost layer has resistivity > 100 Ωm. The second layer has a low resistivity layer of < 10 Ωm with a thickness of roughly 1km, and the third layer has a relatively high resistivity of >80 Ωm.

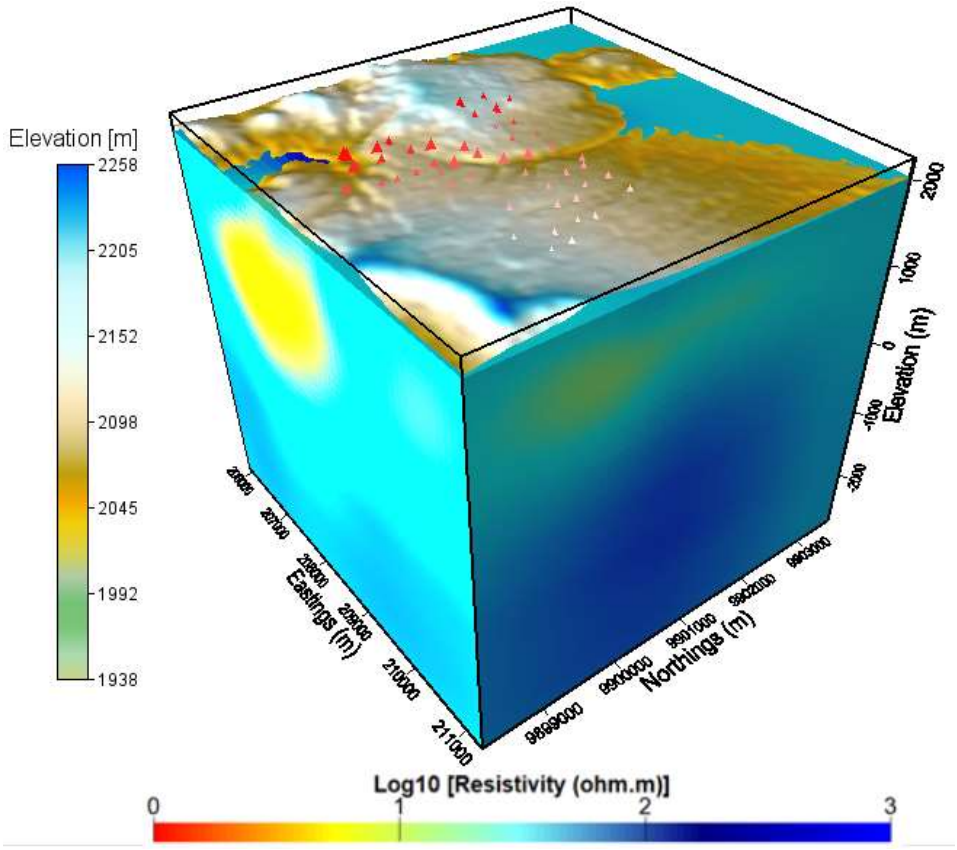

Figure 4.15: 3D Resistivity Model of the Eastern Side of the Olkaria Domes

In the 3D inversion, two profiles passing through the same sounding used for 2D inversion were analyzed. In both profiles, there is a conductive layer of 5–10 Ωm at around 2–2.5 km and a very resistive layer close to the surface with a thickness of approximately 1 km. A comparatively high resistive zone of > 80 Ωm lies below the conductive layer. A highly resistant layer lies beneath, with a resistivity > 100 Ωm from around 4 km to 5 km.

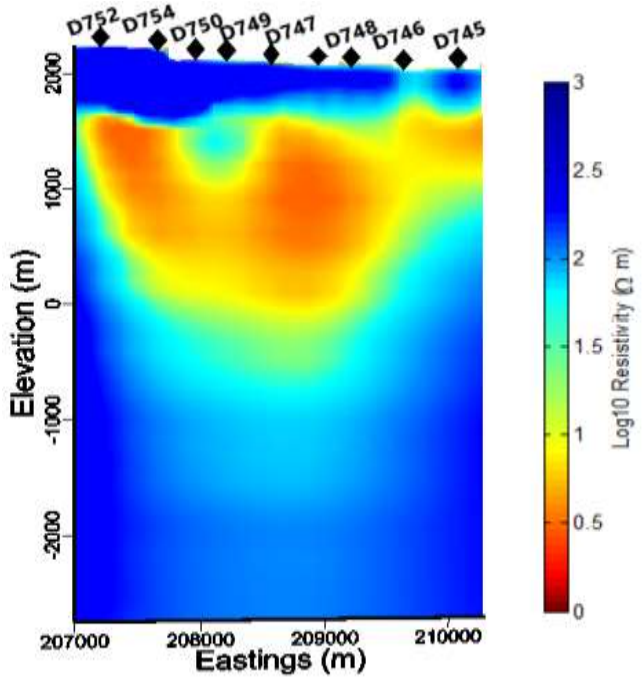

Figure 4.16: 3D Resistivity Model for Profile 1

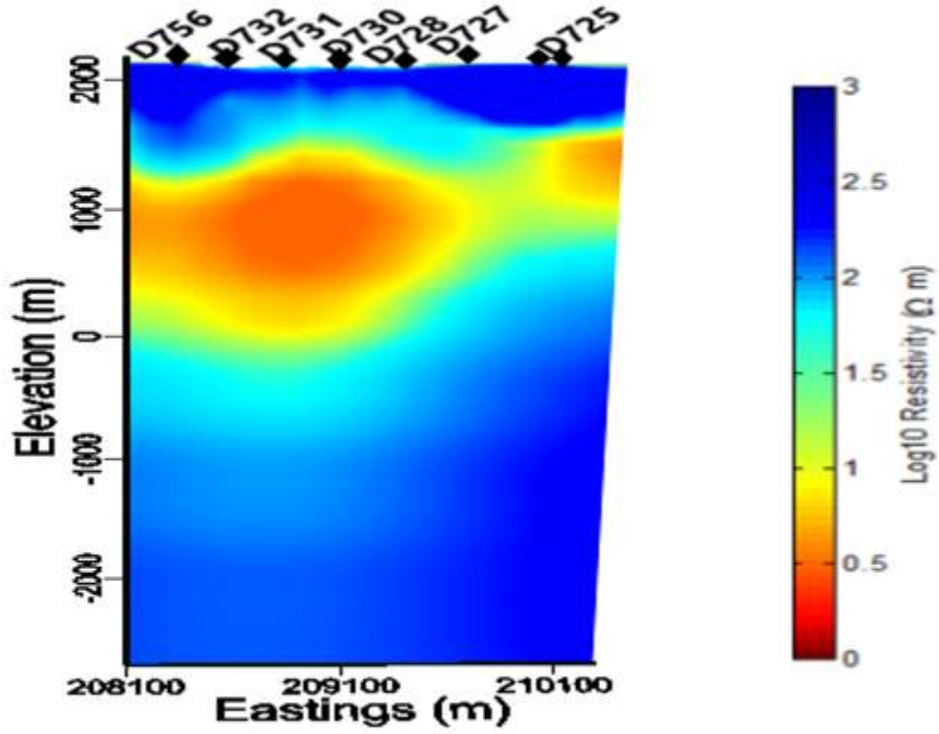

Figure 4.17: 3D Resistivity Model for Profile 2

The iso-resistivity surface (30 Ωm) that represents a possible geothermal reservoir lies above a very high resistive layer obtained from the inversion (Figure 4.18).

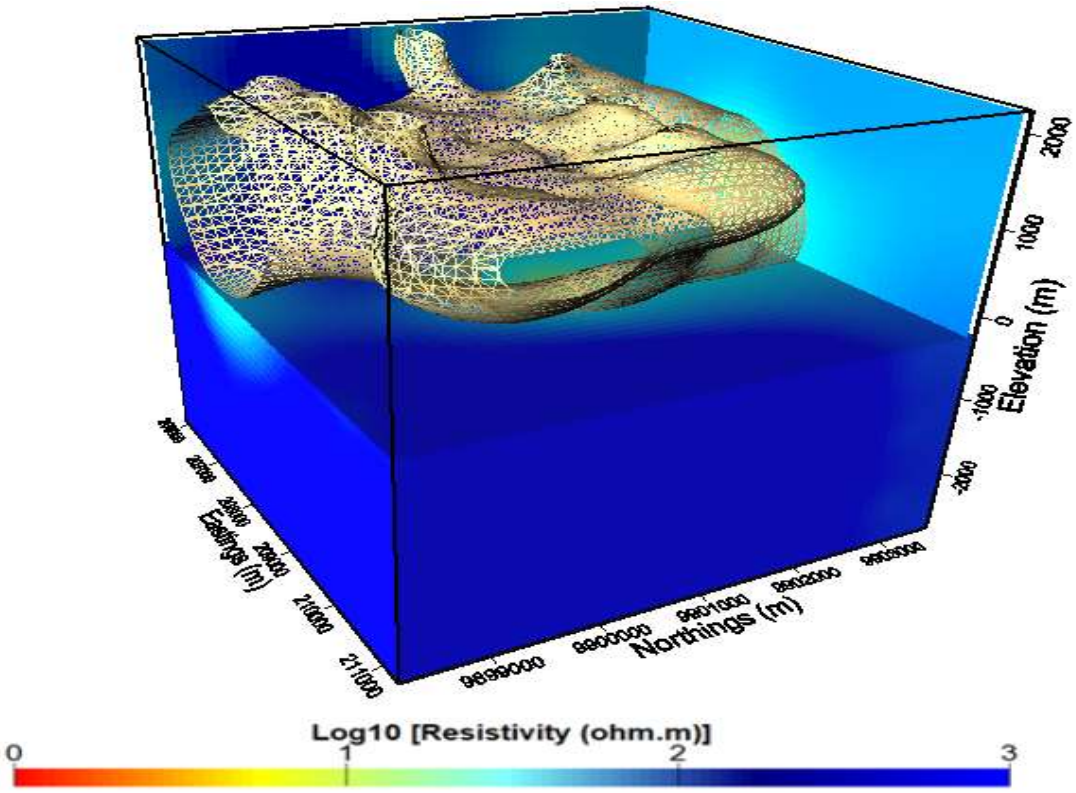

Figure 4.18: 3D Resistivity Model of the Eastern Side of Olkaria Domes Showing an Iso – Surface of 30 Ωm

4.5.3 Comparison of 2D and 3D Inversion Models

The comparison of the two models (Figure 4.19) shows that the structures identified in profiles 1 and 2 of the 2D model display characteristics similar to those observed in 3D inversion models on the same profiles. However, at depth, the 3D model gives a better resolution of a conductive layer at a depth of 1.5 to 2km with a resistivity of <10 Ωm, which is different from the resistivity mapped by the 2D inversion. Since deep subsurface structures are mostly three-dimensional, the 3D model revealed hidden or exaggerated features present in the 2D model at greater depths.

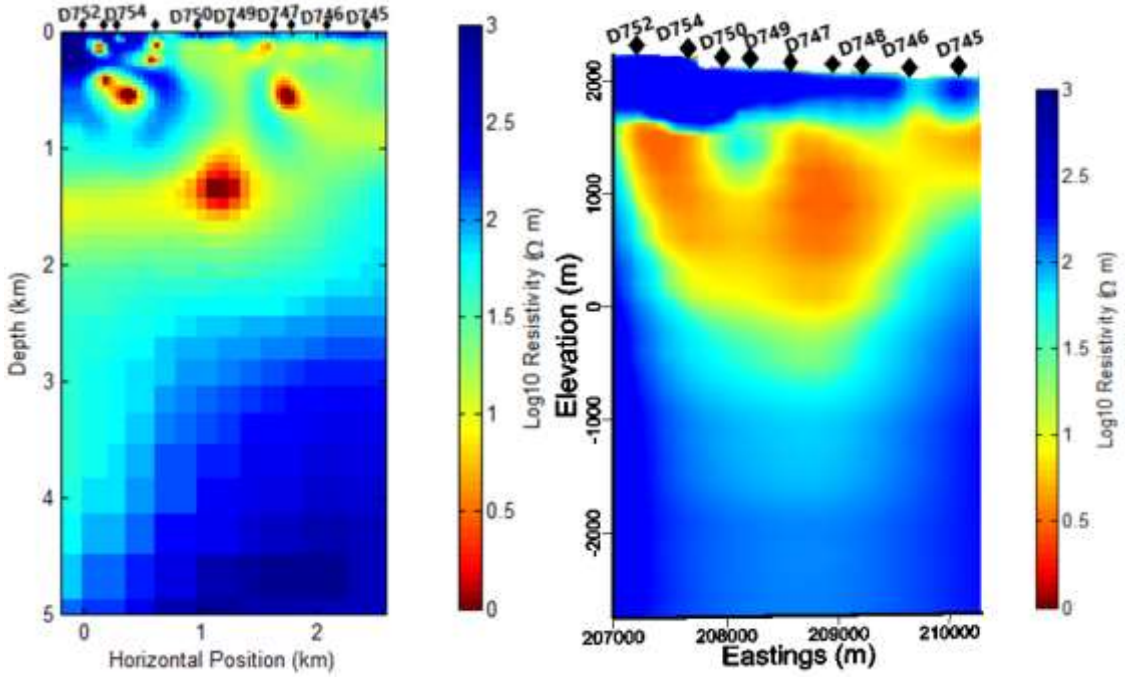

Figure 4.19: 2D and 3D Models for Profile 1, Respectively.

CHAPTER FIVE

CONCLUSIONS AND RECOMMENDATIONS

5.1 Conclusion

MT data analysis was performed in this study to identify subsurface structures on the eastern side of the Olkaria domes. The resistivity models from 2D and 3D inversion revealed three layers that vary with depth. An unaltered formation is the upper, near-surface resistive layer of >100 Ωm, which extends almost to 1 km above sea level. The reservoir seal can be considered to be the second layer, which is a conductive zone of < 10 Ωm. The low resistivity at the reservoir seal is likely to be caused by smectite and illite minerals. The third layer, which has a comparatively high resistivity of > 80 Ωm at a depth of 2.5 to 4 km was interpreted to represent the reservoir zone. The conductive channels observed in the models are probably faults that influence fluid movement and transfer heat from deeper zones to the surface. The resistivity structure of the eastern side of the Olkaria domes highlights features typical of a high-enthalpy geothermal system. Because most geological bodies are 3D structures that MT data responds to, the 3D inversion method provided a better image of the geological structures controlling the geothermal system than the 2D approach. Analysis of two parallel profiles using 3D magnetotelluric inversion indicates a geothermal reservoir area of about 1.5 km^2.

5.2 Recommendations

The study's findings indicate that the geothermal reservoir extent was inferred from a small, sparsely sampled area. I recommend acquiring denser and more comprehensive data to achieve clearer imaging of the geothermal structures.

REFERENCES

Aizawa, K., Koyama, T., Hase, H., Uyeshima, M., Kanda, W., & Utsugi, M., (2014). Three-dimensional resistivity structure and magma plumbing system of the Kirishima Volcanoes as inferred from broadband Magnetotelluric data. J. Geophysics. *Resource. Solid Earth 119*, 198–215. https://doi.org/10.1002/2013JB010682.

Árnason, K., Eysteinsson, H., & Hersir, G.P., (2010). Joint 1-D inversion of TEM and MT data and 3-D inversion of MT data in the Hengill area, SW Iceland. *Geothermics*, *39*(1), 13–34.

Arthur, M.M., (2017) Three Dimensional Inversions of MT Resistivity Data to Image Geothermal Systems: Case Study, Korosi Geothermal Prospect. In *Proceedings, 42nd Workshop on Geothermal Reservoir Engineering Stanford University*, Stanford, California, February 13-15, 2017 SGP-TR-212.

Axelsson, G., Gudmundsdottir, V., Andri, A., Halldor, A., Knútur, A., Hjalti, F., Saeunn, H., & Gylfi, P.H., (2017)**.** Revision of the Conceptual Model for the Olkaria Geothermal System. Proceedings, 42nd Work. Geotherm. Reserve. Eng. Stanford Univ. Stanford, Calif 1–9. Cagniard, L., 1953. In *Basic Theory of the Magnetotelluric Method of Geophysical Prospecting* 18, 603–635. https://doi.org/10.1190/1.1437915.

Bahr, K., (1988). Interpretation of the Magnetotelluric impedance tensor: regional induction and local telluric distortion. *J. Geophysics, 62*, 119-127.

Bahr, K., (1991). Geological noise in Magnetotelluric data: a classification of distortion types, Phys. *Earth planet. Inter., 66*, 24-38.

Berdichevsky, M. N., & Dmitriev, V. I., (1976). Basic principles of interpretation of Magnetotelluric curves, in Geoelectric and Geothermal Studies, pp. 165-221, ed. Á. Adam, KAPG Geophysical Monograph, Akademie Kaido, Budapest.

Berdichevsky, M. N., & Dmitriev, V. I., (2008). *Models and methods of Magnetotelluric.* Springer-Verlag, Berlin Heidelberg, Germany.

Cagniard, L., (1953). Basic theory of the Magnetotelluric method of geophysical prospecting. *Geophysics, 18*, 605-635.

Caldwell, T. G., Bibby, H. M., & Brown, C. (2004). The magnetotelluric phase tensor. *Geophysical Journal International*, *158*(2), 457-469.

Campanya, J., Ogaya, X., Jones, A. G., Rath, V., Vozar, J., & Meqbel, N. (2016). The advantages of complementing MT profiles in 3-D environments with geomagnetic transfer function and interstation horizontal magnetic transfer function data: results from a synthetic case study. *Geophysical Supplements to the Monthly Notices of the Royal Astronomical Society*, *207*(3), 1818-1836.https://doi.org/ 10.1093/gji/ggw357.

Chave, A. D., & Jones, A. G. (Eds.). (2012). *The magnetotelluric method: Theory and practice*. Cambridge University Press. https://doi.org/10.1017/CBO9781139020138. A. Chave and A. Jones (eds.).

Chorowicz, J., (1990). Dynamics of the different basin types in the East African rift. *J. African Earth Sci. 10*, 271–282. https://doi.org/10.1016/0899-5362(90)90060-R.

Clarke, M. C. G., Woodhall, D. G., Allen, D., & Darling, G. (1990). Geological, volcanological and hydrogeological controls on the occurrence of geothermal activity in the area surrounding Lake Naivasha, Kenya.

Cumming, W., & Mackie, R., (2010). Resistivity imaging of geothermal resource using 1D, 2D, and 3D MT inversion and TDEM static shift correction illustrated by a Glass Mountain case history. In *Proceedings World Geothermal Congress*, pp. 25-29.

Cumming, W., (2009). Geothermal resource conceptual models using surface exploration data. In *Proceedings, Thirty-Fourth Workshop on Geothermal Reservoir Engineering,* Stanford University, Stanford, CA.

Degroot-Hedlin, C., & Constable, S., (1990). Occam's inversion to generate smooth, two-dimensional models from Magnetotelluric data. *Geophysics 55,* 1613–1624. https:// doi.org/10.1190/1.1442813.

Didana, Y.L., Thiel, S., & Heinson, G., (2015). Three-dimensional conductivity model of the Tendaho high enthalpy geothermal field, NE Ethiopia. *J. Volcanol. Geotherm. Res. 290*, 53–62. https://doi.org/10.1016/j.jvolgeores.2014.11.013.

Dupis, A., (1997). A third of a century of Magnetotelluric, The leading Edge, 16, 497-502.

Egbert, G. D., & Kelbert, A. (2012). Computational recipes for electromagnetic inverse problems. *Geophysical Journal International, 189*(1), 251-267.

Fantaye, T. (2010). Magnetotelluric and transient electromagnetic methods in geothermal exploration with examples from the Krysuvik area, SW-Iceland. *United Nations University 'Geothermal Training Programme'reports*, *12*, 151-182.

Gerard. M., Weckmann. U., Josef. P., Kováčiková. S., & Klanica. R., (2018). Regional two-dimensional magnetotelluric profile in West Bohemia/Vogtland reveals deep conductive channel into the earthquake swarm region. *Tectonophysics*, *727*, 1-11.

Hersir, G. P., Björnsson, G., Björnsson, A., & Eysteinsson, H. (1990). Volcanism and geothermal activity in the Hengill area. Geophysical exploration: Resistivity data.

Jiracek, G., (1990). Near-surface and topographic distortions in electromagnetic induction. *Survey. Geophysics, 11, 163-203.*

Johnston, J., Pellerin, L. & Hohmann, G., (1992). Evaluation of electromagnetic methods for geothermal reservoir detection. *Transactions Geothermal Resources Council, 16*, 241–245.

Jones, A., (1988). Static shift of magnetotelluric data and its removal in a sedimentary basin environment. *Geophysics, 53*(7), 967-978.

Kelbert, A., Meqbel, N., Egbert, G. D., & Tandon, K. (2014). ModEM: A modular system for inversion of electromagnetic geophysical data. *Computers & Geosciences*, *66*, 40-53.https:// doi.org/10.1016/j.cageo.2014.01.010.

Lichoro, C. M., (2010). Joint 1-D inversions of TEM and MT data from the Olkaria domes geothermal area, Kenya. *Trans. Geothermal. Resource. Council. 34*(2), 802-808.

Maithya J & Fujimitsu Y., (2019). Analysis and interpretation of Magnetotelluric data in the characterization of the geothermal resource in Eburru geothermal field, Kenya. *Geothermics, 81*(2019) 12-13.

Marshall, A.S., Hinton, R.W., & Macdonald, R., (1998). Phenocrystic fluorite in peralkaline rhyolites. Olkaria, Kenya Rift Valley. Mineral. *Magnetotelluric, 62*, 477–486. https://doi.org/ 10.1180/002646198547855.

Martí, A., Queralt, P., Ledo, J., & Farquharson, C. (2010). Dimensionality imprint of electrical anisotropy in magnetotelluric responses. *Physics of the Earth and Planetary Interiors, 182*(3-4), 139-151.

Marwan., Yanis M., Rinaldi I., & Ismail N., (2019). 2d inversion and static shift of MT and TEM data for imaging the geothermal resources of Seulawah Agam Volcano, Indonesia. *International Journal of GEOMATE, 17*(62), 173–180

Meqbel, N. M. M. (2009). *The electrical conductivity structure of the Dead Sea Basin derived from 2D and 3D inversion of magnetotelluric data* (Doctoral dissertation).

Moorkamp, M. (2007). Comment on 'the magnetotelluric phase tensor'by T. Grant Caldwell, Hugh M. Bibby and Colin Brown. *Geophysical Journal International*, *171*(2), 565-566.

Munoz, G., 2014. Exploring geothermal resources with electromagnetic methods, Survey. *Geophysics, 35*(1), 101–122.

Munyiri, S. K. (2016). *Structural mapping of Olkaria Domes geothermal field using geochemical soil gas surveys, remote sensing and GIS* (Doctoral dissertation).

Mwangi, A. W., (2018). Dimensionality Analysis of the Olkaria Geothermal Field, East Africa Rift.

Naylor, W. I., (1972). Geology of Eburru and Olkaria geothermal prospects. UNDP/EAPL geothermal exploration report.

Newman, G. A., Gasperikova, E., Hoversten, G. M., & Wannamaker, P. E. (2008). Three-dimensional magnetotelluric characterization of the Coso geothermal field. *Geothermics, 37*, 369-399

Ofwona, C., Omenda, P., Mariita, N., Wambugu, J., Mwawongo, G., & Kubo, B., (2006). Surface geothermal exploration of Korosi and Chepchuk prospects. KenGen, Kenya, internal report, 44 pp.

Omenda, P.A., (1998). The geology and structural controls of the Olkaria geothermal system. Kenya. *Geothermics 27,* 55–74. https://doi.org/10.1016/S0375-6505(97)00028-X.

Omollo, P., Nishijima, J., Fujimitsu, Y., & Sawayama, K. (2022). Resistivity structural imaging of the Olkaria Domes geothermal field in Kenya using 2D and 3D MT Data inversion. *Geothermics*, *103*, 102414.

Oskooi, B., Pedersen, L. B., Smirnov, M., Árnason, K., Eysteinsson, H., Manzella, A., & DGP Working Group. (2005). The deep geothermal structure of the Mid-Atlantic Ridge deduced from MT data in SW Iceland. *Physics of the Earth and Planetary Interiors*, *150*(1-3), 183-195.

Otieno, V. O. (2016). *Borehole Geology and sub-surface petrochemistry of the Domes area, Olkaria geothermal field, Kenya, in relation to well OW-922*. United Nations University.

Otieno, V., & Kubai, R. (2013). Borehole geology and hydrothermal mineralisation of well OW-37A, Olkaria east geothermal field, Kenya. *UNU-GTP, Iceland, report*, *2*, 105.

Parasnis, D. S. (2012). *Principles of applied geophysics*. Springer Science & Business Media.

Pellerin, L., Johnston, J. M., & Hohmann, G. W. (1996). A numerical evaluation of electromagnetic methods in geothermal exploration. *Geophysics*, *61*(1), 121-130.

Phoenix Geophysics, (2005). Data Processing User Guide, Phoenix Geophysics Limited, 3781 Victoria Park Avenue, Unit 3, Toronto, ON Canada M1W 3K5.

Samrock, F., Grayver, A. V., Bachmann, O., Karakas, Ö., & Saar, M. O. (2021). Integrated magnetotelluric and petrological analysis of felsic magma reservoirs: Insights from Ethiopian rift volcanoes. *Earth and Planetary Science Letters*, *559*, 116765.https://doi.org/ 10.1016/j.epsl.2021.116765.

Simpson, F., & Bahr K., (2005). *Practical Magnetotelluri*c; Cambridge University Press, Cambridge, https://doi.org/ 10.1017/CBO9780511614095.

Swift, C., (1967). *A Magnetotelluric Investigation of an electrical conductivity anomaly in the Southern United States.* Ph.D. Thesis, Dep. of Geol. And Geophys., Mass. Inst. of Technol., Cambridge.

Telford, W.M., Geldart, L.P., & Sheriff, R.E., (1990). *Applied Geophysics*. Cambridge University press, Cambridge.

Tikhonov, A. N. (1951). *Determination of the electrical characteristics of the deep strata of the Earth's crust*. Scientific Information Centre.

Ussher, G., Harvey, C., Johnstone, R. & Anderson, E., (2000). Understanding the resistivities observed in geothermal systems. In *Proceedings World Geothermal Congress*, pp. 1915–1920.

Ye, T., Huang, Q., Chen, X., Zhang, H., Chen, Y. J., Zhao, L., & Zhang, Y. (2018). Magma chamber and crustal channel flow structures in the Tengchong volcano area from 3-D MT inversion at the intracontinental block boundary southeast of the Tibetan Plateau. *Journal of Geophysical Research: Solid Earth*, *123*(12), 11-112. https://doi.org/10.1029/2018 JB015936, 11,112–11,126.

APPENDICES

Appendix I: Static Shift and Distortion Removal Curves

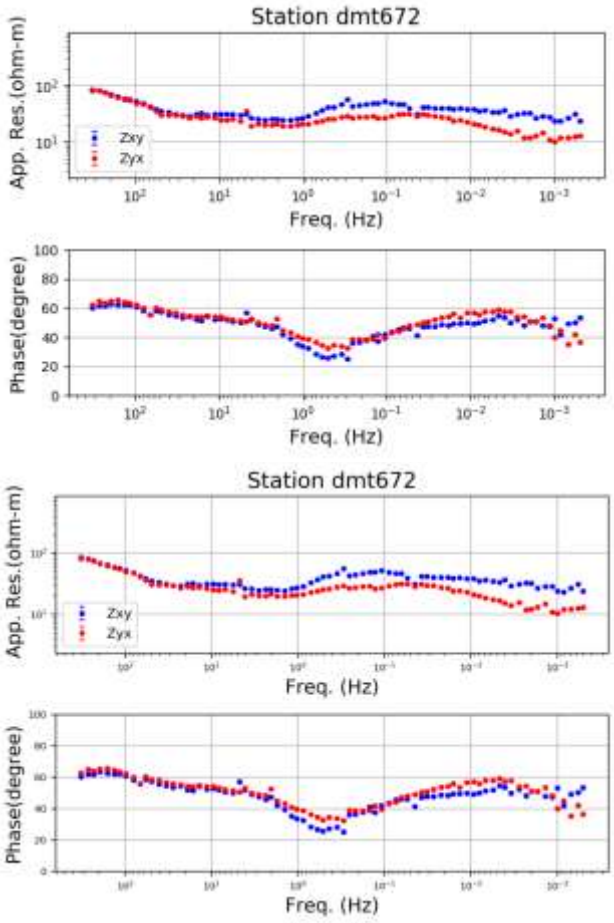

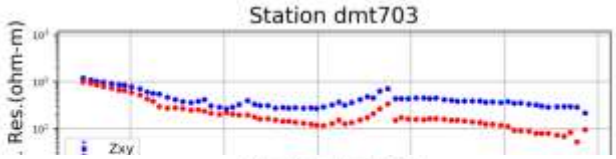
Station dmt703
App. Res.(ohm-m)
Zxy

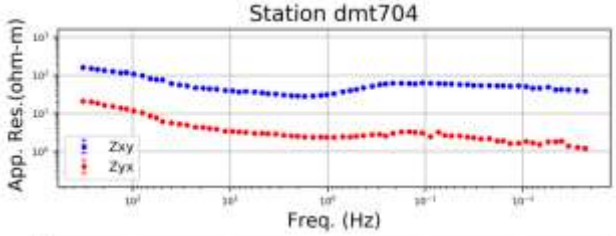
Station dmt704
App. Res.(ohm-m)
Zxy
Zyx
Freq. (Hz)

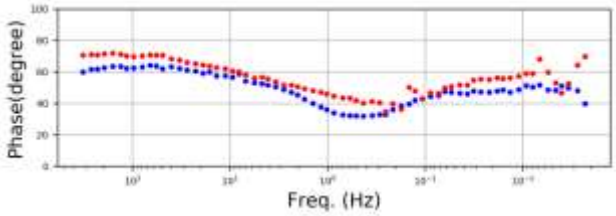
Phase(degree)
Freq. (Hz)

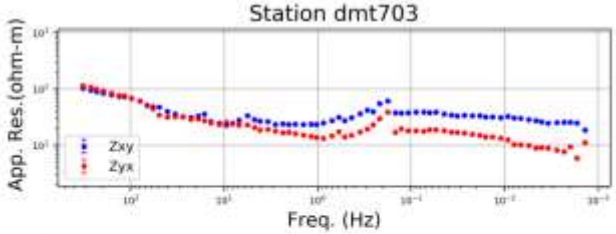
Station dmt703
App. Res.(ohm-m)
Zxy
Zyx
Freq. (Hz)

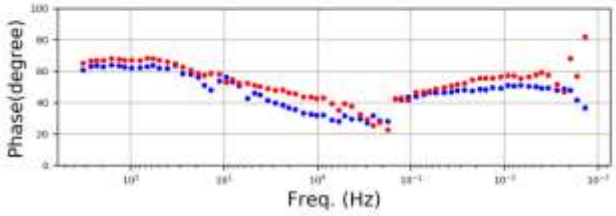
Phase(degree)
Freq. (Hz)

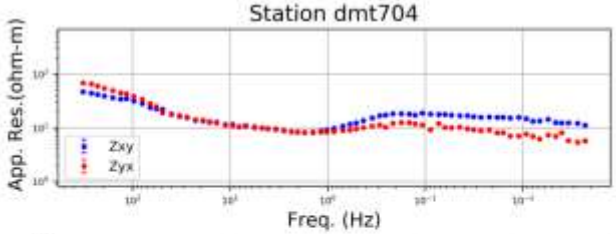
Station dmt704
App. Res.(ohm-m)
Zxy
Zyx
Freq. (Hz)

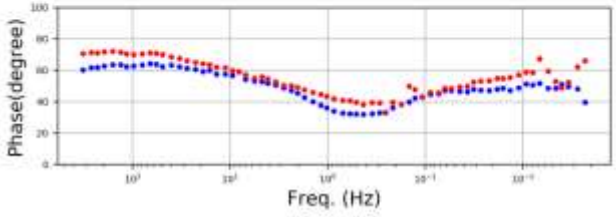
Phase(degree)
Freq. (Hz)

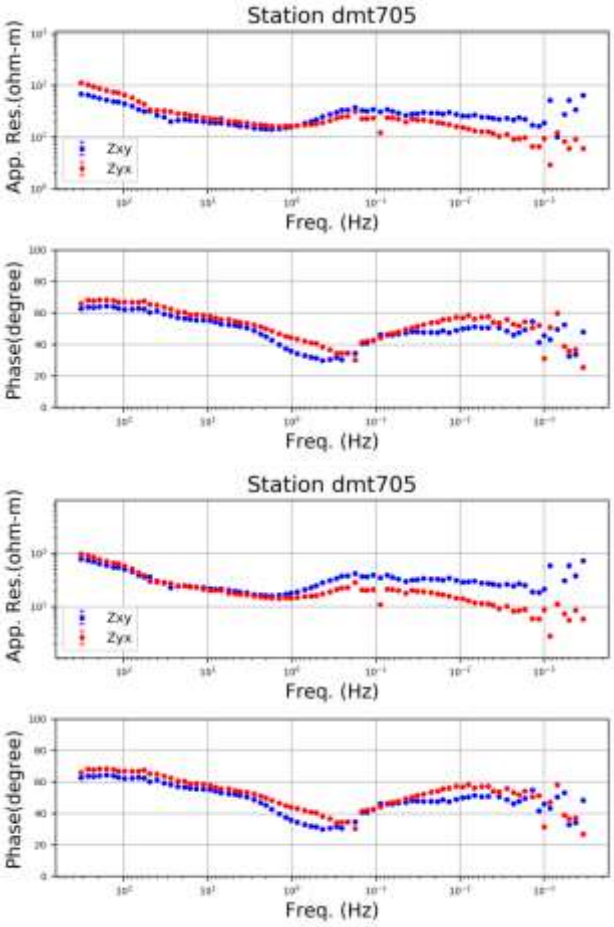
Station dmt705
App. Res.(ohm-m)
Zxy
Zyx
Freq. (Hz)
Phase(degree)
Freq. (Hz)

Station dmt705
App. Res.(ohm-m)
Zxy
Zyx
Freq. (Hz)
Phase(degree)
Freq. (Hz)

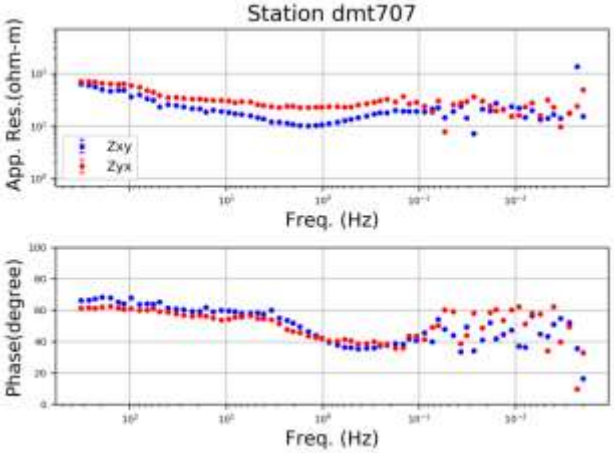
Station dmt707
App. Res.(ohm-m)
Zxy
Zyx
Freq. (Hz)
Phase(degree)
Freq. (Hz)

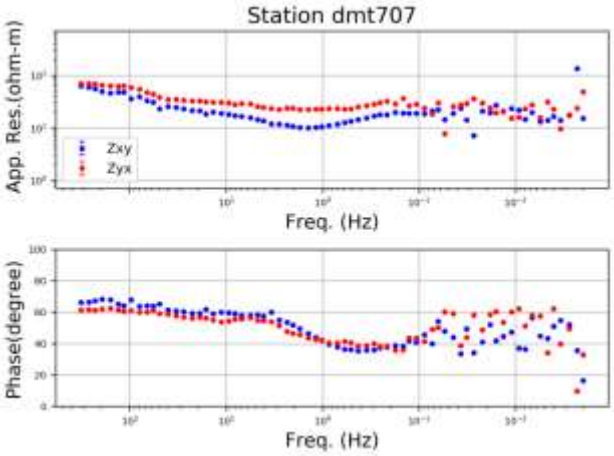
Station dmt707
App. Res.(ohm-m)
Zxy
Zyx
Freq. (Hz)
Phase(degree)
Freq. (Hz)

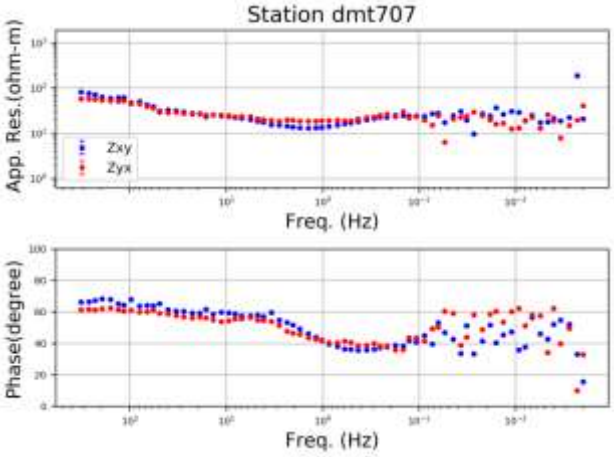
Station dmt707
App. Res.(ohm-m)
Zxy
Zyx
Freq. (Hz)
Phase(degree)
Freq. (Hz)

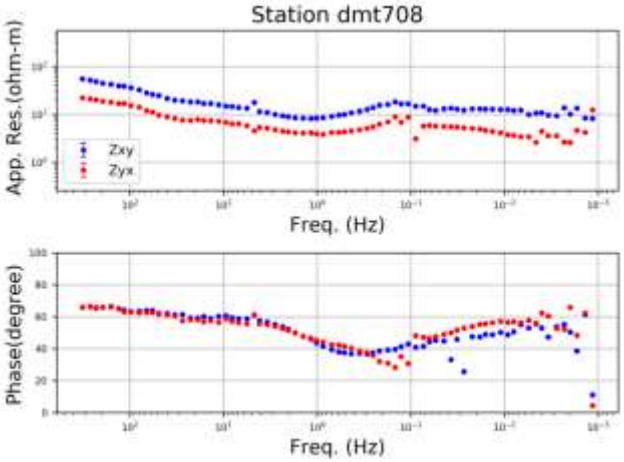
Station dmt708
App. Res.(ohm-m)
Zxy
Zyx
Freq. (Hz)
Phase(degree)
Freq. (Hz)

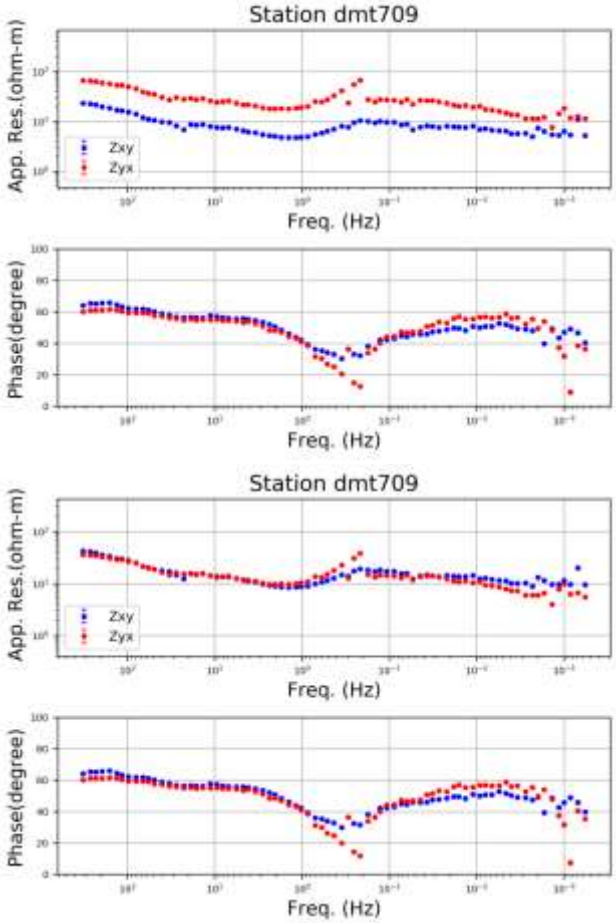
Station dmt709
App. Res.(ohm-m)
Zxy
Zyx
Freq. (Hz)
Phase(degree)
Freq. (Hz)
Station dmt709
App. Res.(ohm-m)
Zxy
Zyx
Freq. (Hz)
Phase(degree)
Freq. (Hz)

Appendix II: Data Misfit Curves

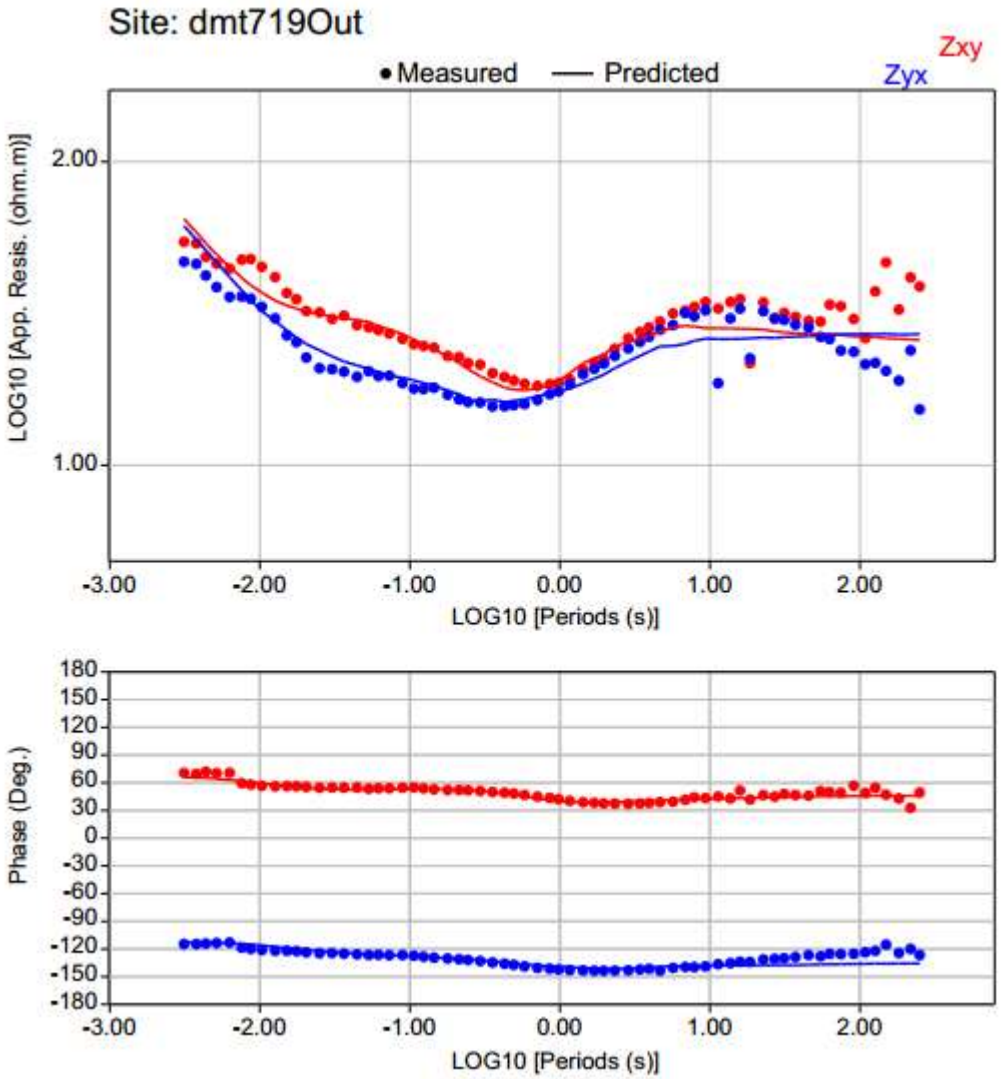

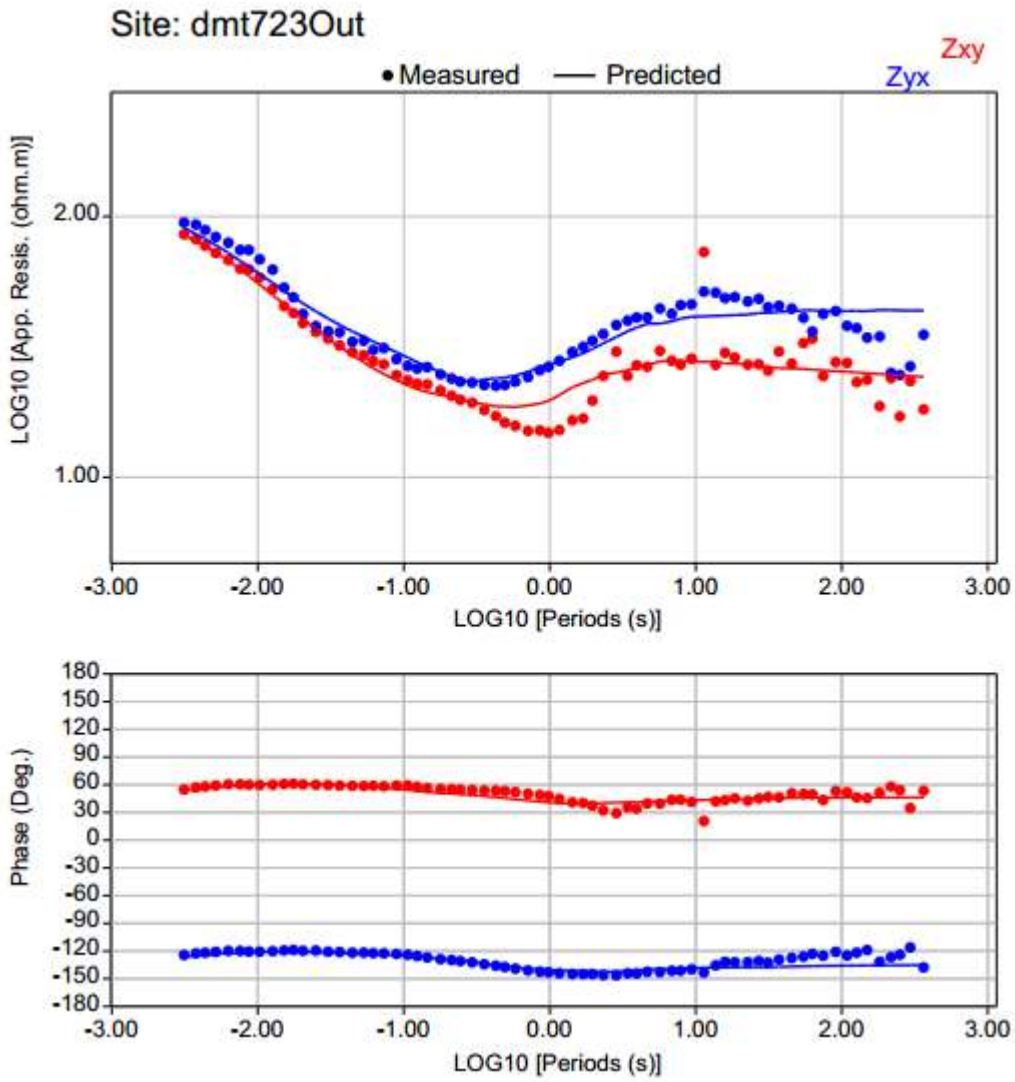
Site: dmt723Out
Measured
Predicted
Zxy
Zyx
LOG10 [App. Resis. (ohm.m)]
2.00
1.00
-3.00
-2.00
-1.00
0.00
1.00
2.00
3.00
LOG10 [Periods (s)]
Phase (Deg.)
180
150
120
90
60
30
0
-30
-60
-90
-120
-150
-180
-3.00
-2.00
-1.00
0.00
1.00
2.00
3.00
LOG10 [Periods (s)]